Supplementary Materials: Applying Screw Theory to Design the Turmell-Bot: a Cable-Driven, Reconfigurable Ankle Rehabilitation Parallel Robot.

Julio H. Vargas-Riaño [1,*], Óscar Agudelo-Varela [2,†] and Ángel Valera [3,†]

S1. Design Formulas

S1.1. Ankle Model

For obtaining the ankle joint model, we used data from anthropometric studies. The values of K, L, O, P, Q with W, and w ratio with standard deviation are in the Table S1.

Table S1. Mean anthropometric values.

Variable	K (mm)	L (mm)	O (mm)	P (mm)	Q (mm)	R = W/w
Mean value	12	16	11	-1	5	0.54

We show the graphical representation in the Figure S1. The figure shows the malleolus most lateral point (MLP), and malleolus mos medial point (MMP). The other values are Q, W, and w. M_1, M_2 pertain to the talocalcaneal axis; N_1 and N_2 to the subtalar axis.

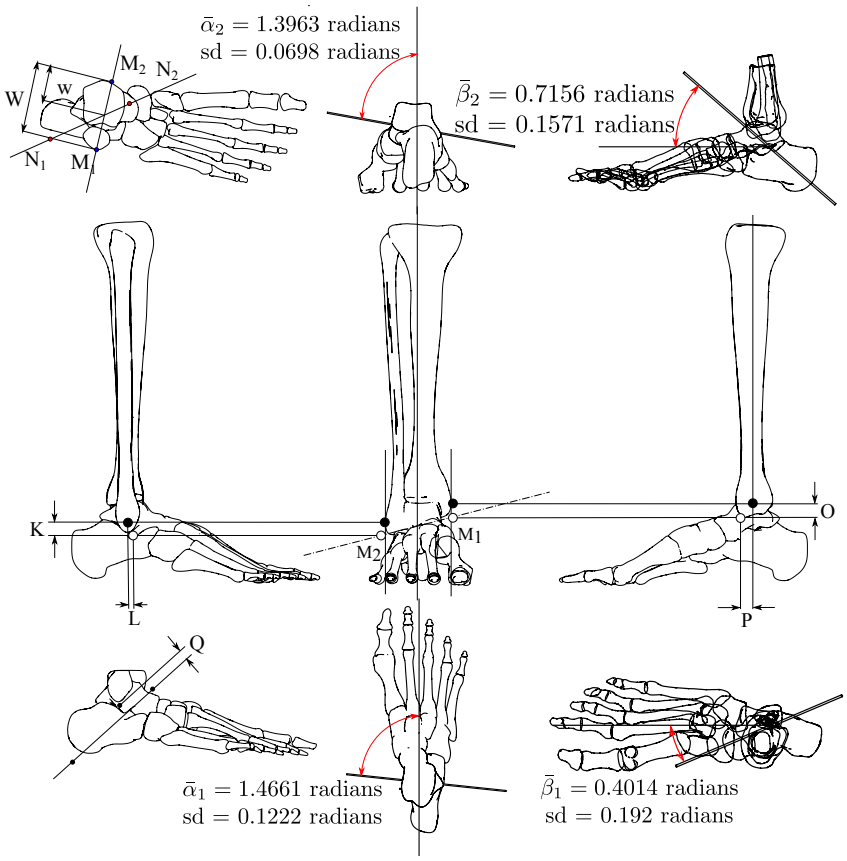

Figure S1. Ankle anthropometric data.

The vectors representing the talocrural and talocalcaneal axis can be reflected about the plane y=0 by using the following equation.

$$\mathrm{Ref}_{\hat{n}}(\hat{v}) = \hat{v} - 2\frac{\hat{v}\cdot\hat{n}_j}{\hat{n}_j\cdot\hat{n}_j}\hat{n}_j. \tag{S1}$$

Where $\hat{n}_j$ is the unitary column vector:

$$\hat{n}_j = [0,1,0]^T, \tag{S2}$$

yielding

$$\mathrm{Ref}_{\hat{n}}(\hat{v}) = \hat{v} - 2(\hat{v}\cdot\hat{n}_j)\hat{n}_j = \left[v_x, -v_y, v_z\right]^T, \tag{S3}$$

which have the matrix representation:

$$R_{xz} = I - 2\frac{\hat{n}_j\cdot\hat{n}_j^T}{\hat{n}_j^T\hat{n}_j} \tag{S4}$$

Replacing the unitary vector $\hat{j}$, the resulting reflection matrix is:

$$R_{xz} = \begin{bmatrix} 1 & 0 & 0 \\ 0 & -1 & 0 \\ 0 & 0 & 1 \end{bmatrix} \tag{S5}$$

Then, by multiplying all the right ankle axis vectors by this matrix, we obtain the left foot kinematic model.

In a single plot, the subtalar axis example trajectories capture method is demonstrated in Figure S2.

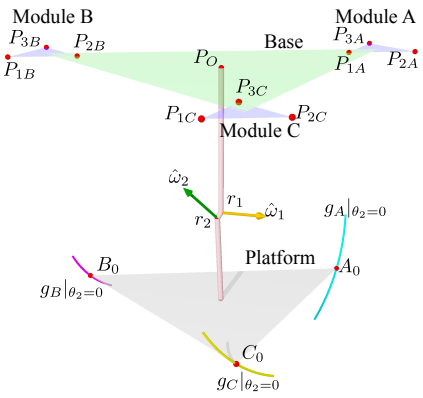

Figure S2. Trajectories capture method.

S1.2. Synthetic Trajectories Generation

In case of the talocrural axis estimation, the trajectories are by plantarflexion and dorsiflexion movements. This means that by blocking the subtalar mobility, the exponential factor will be constant or zero, regarding the initial position election. Assuming the product of exponential formula yields:

$$g_A\ |_{\theta_2=0} = e^{\hat{\xi}_1\theta_1} g_A(0) \tag{S6}$$

Which is a single parameter equation. It corresponds to a circle in the space. We generate the trajectory in the range $\theta_1 \in [-0.3491, 0.3491]$ radians. We also generate artificial

trajectories for the subtalar axis, which is done by replacing the angle, and evaluating for $\theta_2 \in [-0.1745, 0.1745]$ radians. Following that, we obtain:

$$g_A \mid_{\theta_1=0} = e^{\hat{\xi}_2 \theta_2} g_A(0) \tag{S7}$$

S1.3. Platform Position

The schematic model is in the Figure S3. It has three base triangles and three attaching points to the foot's platform. For each point, A, B, and C, we compute the localization in the same way.

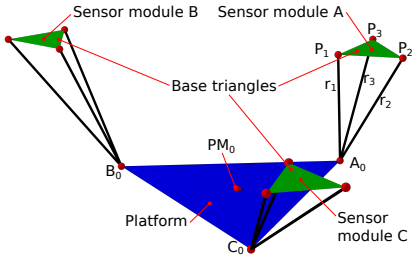

Figure S3. Capturing the platform position.

In the figure, we represent three spheres with centers A, B, and C on the plane $z = 0$. Also, we represented the distances r_1, r_2, and r_3 measured by each sensor. We translated each equilateral triangle to the origin, then, the vertexes are $P_1 = [r_t, 0, 0]$, $P_2 = \left[-\frac{1}{2}, r_t, \frac{1}{2}, \sqrt{3}r_t, 0\right]$, and $P_3 = \left[-\frac{1}{2}, r_t, -\frac{1}{2}, \sqrt{3}r_t, 0\right]$. Where r_t is the radius from each module center to his vertexes. The sphere's radius in each module is r_1, r_2, and r_3, then the equations are:

$$S_1 : (r_t - x)^2 + y^2 + z^2 - r_1^2 = 0 \tag{S8}$$

$$S_2 : \frac{1}{4}(r_t + 2x)^2 + \frac{1}{4}\left(\sqrt{3}r_t - 2y\right)^2 + z^2 - r_2^2 = 0 \tag{S9}$$

$$S_3 : \frac{1}{4}(r_t + 2x)^2 + \frac{1}{4}\left(\sqrt{3}r_t + 2y\right)^2 + z^2 - r_3^2 = 0 \tag{S10}$$

By subtracting the sphere equations S_1 from S_2, S_3 from S_1, and S_3 from S_2, we obtain the planes:

$$P_{12} : -3r_t x + \sqrt{3}r_t y - r_1^2 + r_2^2 = 0 \tag{S11}$$

$$P_{13} : -3r_t x - \sqrt{3}r_t y - r_1^2 + r_3^2 = 0 \tag{S12}$$

$$P_{23} : -2\sqrt{3}r_t y - r_2^2 + r_3^2 = 0 \tag{S13}$$

Which are all parallel to z-axis. Adding P_{12} and P_{13} we have the plane:

$$P_{123} : -2r_1^2 + r_2^2 + r_3^2 - 6r_t x = 0 \tag{S14}$$

Solving y in the plane P_{23}, we obtain:

$$y = -\frac{\sqrt{3}(r_2^2 - r_3^2)}{6r_t} \tag{S15}$$

And solving for x in plane P_{123} , we obtain:

$$x = -\frac{2r_1^2 - r_2^2 - r_3^2}{6r_t} \tag{S16}$$

Finally, replacing x and y in S_1, and solving for z, we have:
And solving for x in plane P_{123} , we obtain:

$$z = \mp \frac{\sqrt{-r_1^4 + r_1^2 r_2^2 - r_2^4 - r_3^4 - 9r_t^4 + (r_1^2 + r_2^2) r_3^2 + 3(r_1^2 + r_2^2 + r_3^2) r_t^2}}{3r_t} \tag{S17}$$

In the Figure S4, we show an example when $r_t = 2$, $r_1 = 5$, $r_2 = 6$, and $r_3 = 7$

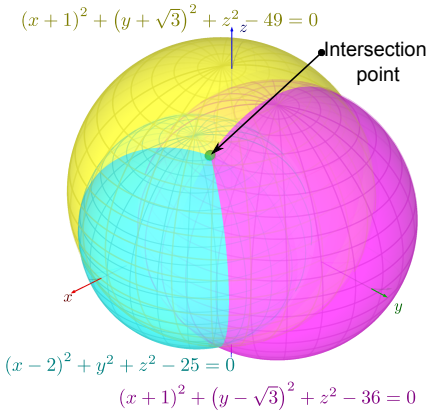

Figure S4. Sphere intersection.

We chose the z-negative value because the origin is over the sensors positions. The Figure S5 shows the geometric representation of the analytic equations.

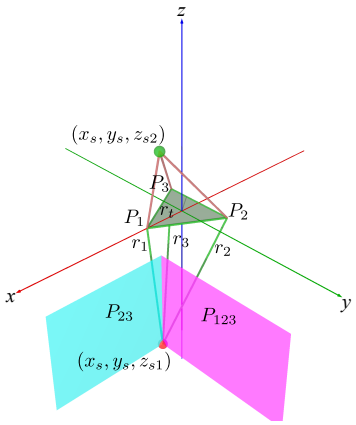

Figure S5. Equations' geometric representation

Finally, we translate the origin to A, B, and C center points at the sensor modules.

S1.4. Selecting the Best Circle-Fitting Trajectories

In this subsection, we select the best measured trajectory. We use draw-wire sensors (DWS). The foot position and orientation can be found from the draw-wire sensors by computing vectors from the measured points A_M, B_M, and C_M.

$$\hat{v}_{AB} = B_M - A_M \tag{S18}$$
$$\hat{v}_{AC} = C_M - A_M \tag{S19}$$

The normal unitary vector is:

$$\hat{n}_v = \frac{\hat{V}_{AB} \times \hat{v}_{AC}}{\|\hat{V}_{AB} \times \hat{v}_{AC}\|} \tag{S20}$$

A unitary vector pointing forward the foot is:

$$\hat{s}_v = \frac{hatV_{AB} + \hat{v}_{AC}}{\|\hat{V}_{AB} + \hat{v}_{AC}\|} \tag{S21}$$

And a perpendicular vector to $\hat{n}_v$ and $\hat{s}_v$ is:

$$\hat{a}_v = \hat{n}_v \times \hat{s}_v \tag{S22}$$

Then, for each instantaneous position, we have a measured transformation matrix:

$$g_M = \begin{bmatrix} s_x & a_x & n_x & p_x \\ s_y & a_y & n_y & p_y \\ s_z & a_z & n_z & p_z \\ 0 & 0 & 0 & 1 \end{bmatrix} \tag{S23}$$

We add two inertial measurement units (IMU), one in the platform and the other in the base. In our design, we use the module GY-6500 with the Invensense's MPU-6500 chip, which integrates a 3-axis gyroscope, a 3-axis accelerometer, and a digital motion processor (DMP). These units have to be first calibrated in a flat surface with the platform coordinates system aligned to the base coordinate's system. The condition for starting and finishing a measured trajectory was carried out by comparing the absolute changes in the accelerometer and the gyroscope.

$$\|a_i - a_{i-1}\| = \|(a_{ix}, a_{iy}, a_{iz}) - \left(a_{(i-1)x}, a_{(i-1)y}, a_{(i-1)z}\right)\| > 0 \tag{S24}$$

$$\|\alpha_i - \alpha_{i-1}\| = \|(\alpha_{ix}, \alpha_{iy}, \alpha_{iz}) - \left(\alpha_{(i-1)x}, \alpha_{(i-1)y}, \alpha_{(i-1)z}\right)\| > 0 \tag{S25}$$

In the real world, we have noise, and the change must be greater than the noise signal. The noise can be estimated during calibration and measuring absolute maximum and minimum values with the accelerometer and the gyroscope in static positions. We subtract the foot and shank measured quaternions:

$$\hat{q}_{SF} = [q_w, q_x, q_y, q_z] = [q_{Fw}, q_{Fx}, q_{Fy}, q_{Fz}] - [q_{Sw}, q_{Sx}, q_{Sy}, q_{Sz}] \tag{S26}$$

And converted the data to angle-axis representation with:

$$\theta = 2 * \arccos(q_w) \tag{S27}$$

$$\omega_x = \frac{q_x}{\sqrt{1 - q_w \cdot q_w}} \tag{S28}$$

$$\omega_y = \frac{q_y}{\sqrt{1 - q_w \cdot q_w}} \tag{S29}$$

$$\omega_z = \frac{q_z}{\sqrt{1 - q_w \cdot q_w}} \tag{S30}$$

For example, we use measurements in A to get a set of points.

$$P_{MA} = [P_{A0}, P_{A1} \ldots P_{An}] \tag{S31}$$

For each point, there is a corresponding IMU attitude:

$$\hat{\omega}_M = [\hat{\omega}_0, \hat{\omega}_1 \ldots, \hat{\omega}_n] \tag{S32}$$

Then, the mean $\bar{\omega}$ of the vector list is perpendicular to the plane containing the circular trajectory.

$$\Pi_C = (\bar{\omega}_x, \bar{\omega}_y, \bar{\omega}_z) \cdot (P - P_{A0}) = 0 \tag{S33}$$

S1.5. Axes Approximation

In this subsection, we used artificial data generated from the anthropometric studies, as an approximation based on real measurements. But the real data will be obtained by using the last subsection method. We briefly describe the method for axis estimation from a selected trajectory containing positions in space. The point positions P_A pertain to a plane Π_A with the equation:

$$Ax + By + Cz + D = 0 \tag{S34}$$

Multiplying this equation by $-\frac{1}{C}$, $C \neq 0$:

$$-\frac{A}{C}x - \frac{B}{C}y - z - \frac{D}{C} = 0 \tag{S35}$$

If we define:

$$a = -\frac{A}{C} \tag{S36}$$

$$b = -\frac{B}{C} \tag{S37}$$

$$d = -\frac{D}{C} \tag{S38}$$

Then, we have:

$$ax + by - z + d = 0, \tag{S39}$$

solving for z on the right side:

$$ax + by + d = z, \tag{S40}$$

The list of the n sample points has the form:

$$\begin{bmatrix} x_0 & y_0 & 1 \\ x_1 & y_1 & 1 \\ \vdots & \vdots & \vdots \\ x_{n-1} & y_{n-1} & 1 \end{bmatrix} \begin{bmatrix} a \\ b \\ d \end{bmatrix} = \begin{bmatrix} z_0 \\ z_1 \\ \vdots \\ z_{n-1} \end{bmatrix} \tag{S41}$$

We define:

$$A_{n\times 3} = \begin{bmatrix} x_0 & y_0 & 1 \\ x_1 & y_1 & 1 \\ \vdots & \vdots & \vdots \\ x_{n-1} & y_{n-1} & 1 \end{bmatrix} \tag{S42}$$

$$x_{3\times 1} = \begin{bmatrix} a \\ b \\ d \end{bmatrix} \tag{S43}$$

$$B_{n\times 1} = \begin{bmatrix} z_0 \\ z_1 \\ \vdots \\ z_{n-1} \end{bmatrix} \tag{S44}$$

Then, the system:

$$A_{n\times 3}x_{3\times 1} = B_{n\times 1} \tag{S45}$$

has the solution:

$$x_{3\times 1} = A^{+}B \tag{S46}$$

where:

$$A^{+} = \left(A^{T}A\right)^{-1}A^{T} \tag{S47}$$

is the pseudo-inverse of $A_{n\times 3}$.

Then we have solved a, b, and d. We replace and solve for A, B, and D in Equations S36, S37, and S38. In the Equation S34, the vector $\hat{N}_{\Pi A} = [A, B, C]$ is perpendicular to the plane Π_A, normalizing the vector, we have:

$$\hat{n}_{\Pi A} = \frac{\hat{N}_{\Pi A}}{\|\hat{N}_{\Pi A}\|} \tag{S48}$$

The angle with the plane $z = 0$, normal to the vector $\hat{k} = [0, 0, 1]$, is given by the dot product equation:

$$\theta_{\hat{n}\to\hat{k}} = \arccos(\hat{n}_{\Pi A} \cdot \hat{k}), \tag{S49}$$

the cross product:

$$\hat{v}_{\hat{n}\perp\hat{k}} = \hat{n} \times \hat{k} \tag{S50}$$

is perpendicular to $\hat{n}_{\Pi A}$ and $\hat{k}$.

Rotating all the points an angle θ_r about the direction vector $\hat{v} = \left[\nu_x, \nu_y, \nu_z\right]$ can be achieved by applying the rotation transformation to each point in the arc:

$$P_R = R_{\hat{v},\theta}P = e^{N\Theta}P \tag{S51}$$

Where:

$$e^{N\Theta} = I_{3\times 3} + N\sin\Theta + N^2(1 - \cos\Theta) \tag{S52}$$

And:

$$N = \begin{bmatrix} 0 & -\nu_z & \nu_y \\ \nu_z & 0 & -\nu_x \\ -\nu_y & \nu_x & 0 \end{bmatrix} \tag{S53}$$

Now the points are in a plane parallel to the plane $z = 0$, then we use the two-dimensional circle equation:

$$(x - x_c)^2 + (y - y_c)^2 = r^2, \tag{S54}$$

expanding the equation yields:

$$x^2 - 2xx_c + x_c^2 + y^2 - 2yy_c + y_c^2 = r^2. \tag{S55}$$

Rearranging:

$$(2x_c)x + (2y_c)y + (r^2 - x_c^2 - y_c^2) = x^2 + y^2, \tag{S56}$$

Which has the form:

$$\chi_0 x + \chi_1 y + \chi_2 = x^2 + y^2, \tag{S57}$$

Where:

$$\chi_0 = 2x_c \tag{S58}$$
$$\chi_1 = 2y_c \tag{S59}$$
$$\chi_2 = r^2 - x_c^2 - y_c^2. \tag{S60}$$

The P_R set of points can be arranged in the system:

$$\begin{bmatrix} x_0 & y_0 & 1 \\ x_1 & y_1 & 1 \\ \vdots & \vdots & \vdots \\ x_{n-1} & y_{n-1} & 1 \end{bmatrix} \begin{bmatrix} \chi_0 \\ \chi_1 \\ \chi_2 \end{bmatrix} = \begin{bmatrix} x_0^2 + y_0^2 \\ x_1^2 + y_1^2 \\ \vdots \\ x_{n-1}^2 + y_{n-1}^2 \end{bmatrix}, \tag{S61}$$

has the form:

$$Ax = B \tag{S62}$$

Which is similar to the Equation S45. We found the vector, and we found the center $c_r = [x_c, y_c]$ and the radius r_f replacing the components in Equations S58, S59 and S60. Then, we rotate back the center C_{rt} using the negative angle $-\Theta_{\hat{n}\to\hat{k}}$, and the same axis $\hat{v}_{\hat{n}\perp\hat{k}}$. We have three generated trajectories by tracking A, B, and C. Then, we averaged the resulting vectors and centers.

$$\bar{v}_{rt} = \frac{1}{3}(v_{rtA} + v_{rtB} + v_{rtC}) \tag{S63}$$
$$\bar{c}_{rt} = \frac{1}{3}(c_{rtA} + c_{rtB} + c_{rtC}) \tag{S64}$$

We applied a similar method for the subtalar axis joint. Finally, the initial axis representation is in Plücker line coordinates.

S1.6. Range of Motion

With the axis estimation from a selected trajectory, we computed the corresponding angles for the different positions. The measured homogeneous transformation matrix in the Equation S1.4 measured rotation matrix.

$$R_M = \begin{bmatrix} s_x & a_x & n_x \\ s_y & a_y & n_y \\ s_z & a_z & n_z \end{bmatrix}, \tag{S65}$$

by using the definition of logarithm matrix, we compute the rotation angles as follows. We take the measured trajectories A_M, B_M, and C_M to compute the vectors $\hat{s}$, $\hat{a}$, and $\hat{n}$ to get the rotation matrix for each set of measurements. For each trajectory set $A_{M(i)}$, $B_{M(i)}$, $C_{M(i)}$ with index i=1 to n measurements. The estimate the angle from the initial position is:

$$\theta_m = \arccos\left(\frac{1}{2}(\mathbf{tr}(R_M) - 1)\right) \in [0, \pi) \tag{S66}$$

Where $\mathbf{tr}(R_M)$ is the trace of the measured matrix R_M. In this equation, the angles must be positive, then we choose two groups of measurements. In the set of computed angles, the zero value divides the table in negative and positive values, we defined θ_{mn} and θ_{mp} , as the negative and positive group of angles. The first group is from the zero position to the maximum value in the negative rotation regarding the rotation axis. The negative maximum angle from the initial position is:

$$\theta_{min} = -\mathbf{max}(\theta_{mn}) \tag{S67}$$

The positive maximum angle from the initial position is:

$$\theta_{min} = \mathbf{max}(\theta_{mp}) \tag{S68}$$

The range of movement (Rom) is the difference between the positive and the negative value.

$$\mathbf{R.O.M.} = \theta_{mp} - \theta_{mn} \tag{S69}$$

This procedure has the same results when we add the two greatest values. We validate the data from the measured rotation matrix with the skew-symmetric matrix:

$$[\hat{\omega}_m] = \frac{1}{2\sin\theta_m}\left(R_M - R_M^T\right) \tag{S70}$$

With the selected trajectories, we prove that the angle identification is correct.

S1.7. Common Perpendicular and its Feet

The lines representing the axes contain two points r_{1C} and r_{2C}, which are the feet of the common perpendicular line between the axes. We used the Plücker line coordinates to find the intersection points with the axis. Then, we represent the lines with six-dimensional vectors:

$$\$_1 = [\hat{\omega}_1, \hat{v}_1] \tag{S71}$$
$$\$_2 = [\hat{\omega}_2, \hat{v}_2] \tag{S72}$$

The common perpendicular components are:

$$\hat{\omega}_C = \hat{\omega}_{1\perp 2} = \hat{\omega}_1 \times \hat{\omega}_2 \tag{S73}$$
$$\hat{v}_C = \hat{v}_{1\perp 2} = \hat{v}_1 \times \omega_2 - \hat{v}_2 \times \hat{\omega}_1 + \frac{(\$_1 \cdot \$_2)(\hat{\omega}_1 \cdot \hat{\omega}_2)}{\|\hat{\omega}_1 \times \hat{\omega}_2\|^2}(\hat{\omega}_1 \times \hat{\omega}_2) \tag{S74}$$

We compute the intersection points between the common perpendicular and the axes with:

$$r_{1C} = r_{1\perp 2} = \frac{-\hat{v}_1 \times [\hat{\omega}_2 \times (\hat{\omega}_1 \times \hat{\omega}_2)] + [\hat{v}_2 \cdot (\hat{\omega}_1 \times \hat{\omega}_2)]\hat{\omega}_1}{\|\hat{\omega}_1 \times \hat{\omega}_2\|^2} \tag{S75}$$

$$r_{2C} = r_{2\perp 1} = \frac{\hat{v}_2 \times [\hat{\omega}_1 \times (\hat{\omega}_1 \times \hat{\omega}_2)] - [\hat{v}_1 \cdot (\hat{\omega}_1 \times \hat{\omega}_2)]\hat{\omega}_2}{\|\hat{\omega}_1 \times \hat{\omega}_2\|^2} \tag{S76}$$

Finally, we have the initial position of the two axes. We use the transverse planes perpendicular to the total tension force in the shank-ankle-foot kinematic chain. For selecting a central point for the attaching points configuration, we found the projection of each axis on the base plane. It is the result of multiplying the orthogonal projection matrix on the base P_b by $\hat{\omega}_1$:

$$P_b = \begin{bmatrix} 1 & 0 & 0 \\ 0 & 1 & 0 \\ 0 & 0 & 0 \end{bmatrix} \cdot \hat{\omega}_1 = [\omega_1 x, \omega_1 y, 0] \tag{S77}$$

Also, we project the vectors, $\hat{\omega}_2$, r_{1C}, and r_{2C}. The resulting projections define two lines, and we define two points pertaining to the talocrural axis in homogeneous representation:

$$P_{1b1} = P_b \cdot \hat{r}_{1C} + \hat{k} \tag{S78}$$

$$P_{1b2} = P_b \cdot (\hat{r}_1 + \hat{\omega}_1) + \hat{k} \tag{S79}$$

And for the subtalar axis:

$$P_{2b1} = P_b \cdot \hat{r}_{2C} + \hat{k} \tag{S80}$$

$$P_{2b2} = P_b \cdot (\hat{r}_2 + \hat{\omega}_2) + \hat{k} \tag{S81}$$

With $\hat{k} = [0, 0, 1]$. Then, by using determinants, the intersection point $P_{ixy} = [P_i x, P_i y, 0]$ components are:

$$P_{ix} = \frac{\begin{vmatrix} D_{1xy} & D_{1x1} \\ D_{2xy} & D_{2x1} \end{vmatrix}}{\begin{vmatrix} D_{1x1} & D_{1y1} \\ D_{2x1} & D_{2y1} \end{vmatrix}} \tag{S82}$$

$$P_{iy} = \frac{\begin{vmatrix} D_{1xy} & D_{1y1} \\ D_{2xy} & D_{2y1} \end{vmatrix}}{\begin{vmatrix} D_{1x1} & D_{1y1} \\ D_{2x1} & D_{2y1} \end{vmatrix}} \tag{S83}$$

Where:

$$D_{1xy} = \begin{vmatrix} P_{1b1x} & P_{1b1y} \\ P_{1b2x} & P_{1b2y} \end{vmatrix} \tag{S84}$$

$$D_{2xy} = \begin{vmatrix} P_{2b1x} & P_{2b1y} \\ P_{2b2x} & P_{2b2y} \end{vmatrix} \tag{S85}$$

And:

$$D_{1x1} = \begin{vmatrix} P_{1b1x} & 1 \\ P_{1b2x} & 1 \end{vmatrix} \quad \text{(S86)}$$

$$D_{1y1} = \begin{vmatrix} P_{1b1y} & 1 \\ P_{1b2y} & 1 \end{vmatrix} \quad \text{(S87)}$$

$$D_{2x1} = \begin{vmatrix} P_{2b1x} & 1 \\ P_{2b2x} & 1 \end{vmatrix} \quad \text{(S88)}$$

$$D_{2y1} = \begin{vmatrix} P_{2b1y} & 1 \\ P_{2b2y} & 1 \end{vmatrix} \quad \text{(S89)}$$

The reference frames on the base P_O and the platform P_{M0} are related to the ankle kinematic chain reference frames P_{Oi} and P_{M0i} by:

$$P_{Oi} = P_O + P_{ixy} \quad \text{(S90)}$$

$$P_{M0i} = P_{M0} + P_{ixy} \quad \text{(S91)}$$

We obtain values for P_{Oi}, P_{M0i}, r_{1C}, r_{2C}, $\hat{\omega}_1$, and $\hat{\omega}_2$. The kinematic chain starts from P_{Oi}, followed by a hinge joint at r_{1C}, then a perpendicular segment to a hinge joint at r_{2C}, ending in the platform center $PM0i$. In summary, we obtained a simplified model for the shank-ankle-foot kinematic chain. We show the kinematic chain, the base, and the platform in Figure S6.

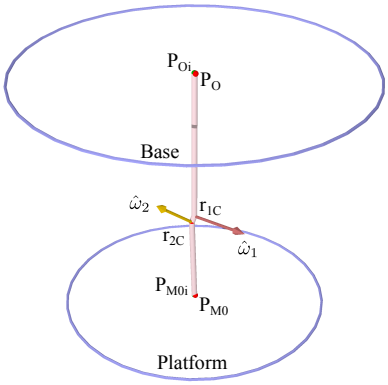

Figure S6. Shank-ankle-foot kinematic chain with base and platform in initial position.

In the figure, the platform radius and base radius are arbitrary, and in the next section we evaluate the base and the platform sizes for avoiding collision with the body. The radius must be smaller than the sensor base and platform, and will be used for configuring the cable-attaching points.

S2. Synthetic Data for Validation

S2.1. Ankle Forward Kinematics

There are two reference systems, the base with origin $P_O = (0, 0, 0)$ and the platform, with origin $P_M = (0, 0, zp)$ at the platform center. The initial points are in Table S2.

Table S2. Platform's initial position.

Platform radius r_p	Origin distance z_p	Initial Point A_0	Initial Point B_0	Initial Point C_0
11.57	17.62	(-11.57, 0.0000, -17.62)	(5.785, 10.02, -17.62)	(5.785, -10.02, -17.62)

* units in cm.

The point PM_0 is the mean value from A_0, B_0, and C_0. The mean values from the sample anthropometric measurements and the resulting values for r_1, M_1, M_2 are in Table S3.

Table S3. Talocrural axis approximation.

Foot width	r_1	M_1	M_2
96.42	(0,0,-107.81)	(5.359, -50.99, -116.9)	(-4.565, 43.44, -100.1)

[1] units in mm.

And, for r_2, N_1, N_2 are in Table S4.

Table S4. Subtalar axis approximation.

Foot length	r_2	N_1	N_2
266.5	(3.2803, 0, -111.58)	(-95.07, -27.70, -197.1)	(101.6, 27.70, -26.09)

[1] units in mm.

In this context, we have the points r_1, M_1, and M_2 pertaining to the talocrural axis. Also, r_2, N_1, and N_2 pertain to the subtalar axis. We show the initial configuration in Figure S7.

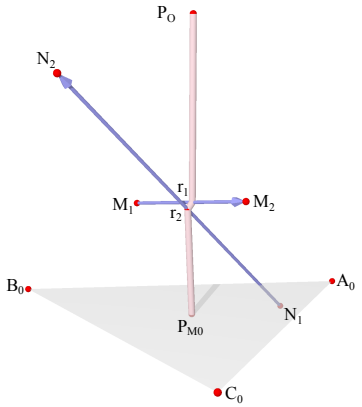

Figure S7. Platform with serial chain and rotation axes at initial position.

We used the mean values for α_1, α_2, β_1, β_1 from Table S5.

Table S5. Mean values for the axis attitude.

Angle Identifier	Mean (radians)
α_1	0.1047
α_2	1.3963
β_1	-0.4014
β_2	0.7156

The resulting vectors for the product of exponentials matrix representation are in Table S6.

Table S6. Vectors for the product of exponentials matrices.

Axis and point	$\hat{\omega}_i$	$\hat{v}_i$
Talocrural on r_1	(-0.103, 0.979, 0.174)	(106., 11.1, 0)
Subtalar on r_2	0.738, 0.208, 0.642)	(23.2, -84.5, 0.682)

The components R_{ij} of the rotation matrix are:

$$\begin{aligned}
R_{11} &= (0.426\cos(\theta_1) - 0.437\sin(\theta_1) + 0.028)\cos(\theta_2) + (0.06\cos(\theta_1) - 0.315\sin(\theta_1) - 0.06)\sin(\theta_2) \\
&\quad + 0.563\cos(\theta_1) + 0.437\sin(\theta_1) - 0.018 \\
R_{12} &= (-0.057\cos(\theta_1) - 0.296\sin(\theta_1) - 0.095)\cos(\theta_2) + (-0.621\cos(\theta_1) + 0.723\sin(\theta_1) - 0.019)\sin(\theta_2) \\
&\quad + 0.158\cos(\theta_1) + 0.123\sin(\theta_1) - 0.005 \\
R_{13} &= (-0.471\cos(\theta_1) + 0.599\sin(\theta_1) - 0)\cos(\theta_2) + (0.131\cos(\theta_1) + 0.128\sin(\theta_1) + 0.076)\sin(\theta_2) \\
&\quad + 0.489\cos(\theta_1) + 0.38\sin(\theta_1) - 0.015 \\
R_{21} &= (0.12\cos(\theta_1) + 0.03\sin(\theta_1) - 0.273)\cos(\theta_2) + (0.061\cos(\theta_1) - 0.021\sin(\theta_1) + 0.58)\sin(\theta_2) \\
&\quad - 0.019\cos(\theta_1) + 0.143\sin(\theta_1) + 0.172 \\
R_{22} &= (0.046\cos(\theta_1) - 0.04\sin(\theta_1) + 0.91)\cos(\theta_2) + (-0.19\cos(\theta_1) - 0.035\sin(\theta_1) + 0.19)\sin(\theta_2) \\
&\quad - 0.005\cos(\theta_1) + 0.04\sin(\theta_1) + 0.048 \\
R_{23} &= (-0.153\cos(\theta_1) - 0.021\sin(\theta_1) + 0.019)\cos(\theta_2) + (-0.009\cos(\theta_1) + 0.036\sin(\theta_1) - 0.729)\sin(\theta_2) \\
&\quad - 0.016\cos(\theta_1) + 0.124\sin(\theta_1) + 0.15 \\
R_{31} &= (-0.425\cos(\theta_1) - 0.429\sin(\theta_1) - 0.048)\cos(\theta_2) + (-0.31\cos(\theta_1) - 0.066\sin(\theta_1) + 0.102)\sin(\theta_2) \\
&\quad + 0.443\cos(\theta_1) - 0.549\sin(\theta_1) + 0.03 \\
R_{32} &= (-0.2948\cos(\theta_1) + 0.051\sin(\theta_1) + 0.161)\cos(\theta_2) + (0.704\cos(\theta_1) + 0.628\sin(\theta_1) + 0.033)\sin(\theta_2) \\
&\quad + 0.124\cos(\theta_1) - 0.154\sin(\theta_1) + 0.008 \\
R_{33} &= (0.584\cos(\theta_1) + 0.477\sin(\theta_1) + 0.003)\cos(\theta_2) + (0.129\cos(\theta_1) - 0.127\sin(\theta_1) - 0.129)\sin(\theta_2) \\
&\quad + 0.385\cos(\theta_1) - 0.477\sin(\theta_1) + 0.026
\end{aligned} \tag{S92}$$

The components of the translation vector τ_A for A reference point are:

$$\begin{aligned}
\tau_{1A} &= -95.442\cos(\theta_1) - 80.284\sin(\theta_1) + 3.283 + (-20.251\cos(\theta_1) + 13.324\sin(\theta_1) - 3.099)\cos(\theta_2) \\
&\quad + (-15.735\cos(\theta_1) + 29.205\sin(\theta_1) + 2.305)\sin(\theta_2) \\
\tau_{2A} &= 4.364\cos(\theta_1) - 24.931\sin(\theta_1) - 31.244 + (-4.402\cos(\theta_1) - 2.196\sin(\theta_1) + 31.281)\cos(\theta_2) \\
&\quad + (-6.729\cos(\theta_1) + 0.214\sin(\theta_1) - 21.937)\sin(\theta_2) \\
\tau_{3A} &= -81.197\cos(\theta_1) + 93.028\sin(\theta_1) - 113.349 + (12.824\cos(\theta_1) + 20.287\sin(\theta_1) + 5.546)\cos(\theta_2) \\
&\quad + (28.626\cos(\theta_1) + l16.104\sin(\theta_1) - 3.889)\sin(\theta_2)
\end{aligned} \tag{S93}$$

The group of movements for the point A are given by.

$$g_A(\theta_1, \theta_2) = \begin{bmatrix} R_T & \tau_A \\ 0_{1\times 3} & 1 \end{bmatrix} \tag{S94}$$

Where the rotation matrix is:

$$R_T = \begin{bmatrix} R_{11} & R_{12} & R_{13} \\ R_{21} & R_{22} & R_{23} \\ R_{31} & R_{32} & R_{33} \end{bmatrix} \tag{S95}$$

And the translation vector is:

$$\hat{\tau}_A = \begin{bmatrix} \tau_{1A} \\ \tau_{2A} \\ \tau_{3A} \end{bmatrix} \tag{S96}$$

With the range of movement for $\theta_1 \in [-0.3491, 0.3491]$ radians, and $\theta_2 \in [-0.1745, 0.1745]$ radians, we obtain the group of movements for each vertex on the platform. We also apply the same transformation to the group of movements for B, C, and P_M. The Figure S8 shows the resulting group of movements.

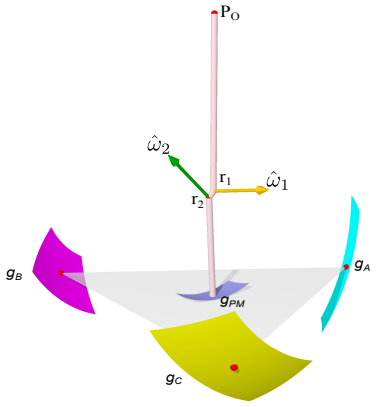

Figure S8. Group of movements for A, B, C, and PM.

We change the talocrural and subtalar axes attitude from the Table S7.

Table S7. Ankle axes attitude modifications.

Angle Identifier	**Maximum** radians	**Minimum** radians
α_1	0.2269	-0.0175
α_2	1.3265	1.4661
β_1	-0.2094	-0.5934
β_2	0.8727	0.5585

We show the resulting $\hat{\omega}_1$ and $\hat{\omega}_2$ values in the Table S8.

Table S8. Direction vectors of the ankle axes.

Group of values	$\hat{\omega}_1$	$\hat{\omega}_2$
Maximum	(0.0174, 0.994, 0.105)	(0.629, 0.208, 0.749)
Minimum	(-0.218, 0.945, 0.242)	(0.703, 0.559, 0.439)

The resulting $\hat{v}_1$ and $\hat{v}_1$ are in Table S9.

Table S9. Momentum for maximum and minimum axis attitude.

Group of values	$\hat{\omega}_1$	$\hat{\omega}_2$
Maximum	(107., -1.87, 0)	(23.1, -72.7, 0.796)
Minimum	(102., 23.5, 0)	(62.7, -79.9, 1.48)

The resulting group of movements for the maximum and minimum values is in the Figure S9 (The figure is in the same camera parameters).

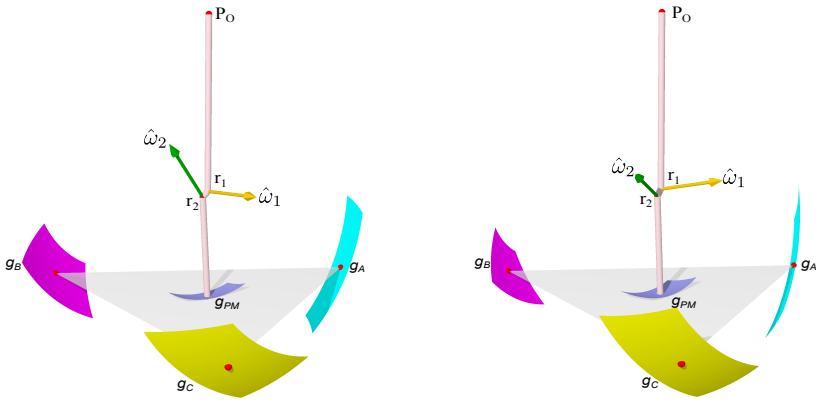

(a) **(b)**

Figure S9. Group of movements SO(3). (**a**) Maximum axes attitude values. (**b**) Minimum axes attitude values.

We also show the data generated from reflection matrix, resulting in artificial data for the left foot. The resulting reflection matrix concerning the $x - z$ sagittal plane is:

$$R_{xz} = \begin{bmatrix} 1 & 0 & 0 \\ 0 & -1 & 0 \\ 0 & 0 & 1 \end{bmatrix}, \tag{S97}$$

The resulting reflected platform initial points are in Table S10.

Table S10. Left foot platform initial points.

A_0 left	B_0 left	C_0 left
(-115.7, 0, -176.18)	(57.849, 100.20, -176.18)	(57.849, -100.20, -176.18)

The talocrural reflected points are in Table S11.

Table S11. Talocrural axis reflected points.

M_1 reflected	M_2 reflected
(5.3595, 50.992, -116.85)	(-4.5655, -43.438, -100.11)

And for the subtalar axis, the resulting reflected points are in Table S12.

Table S12. Subtalar axis reflected points.

N_1 reflected	N_2 reflected
(-95.071, 27.700, -197.08)	(101.63, -27.700, -26.088)

The Figure S10 shows the data generated for the left ankle-foot kinematic model reflected.

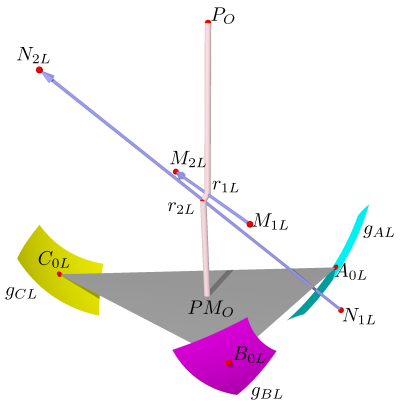

Figure S10. Left foot group of movements.for A, B, C, and PM.

We are able to simulate artificial data from anthropometric studies, and this simplifies our work because we do not have to measure directly in ankle-foots from cadaver specimens. It is an approximated model, but is enough for the device size specification, axis estimation, and validation.

S2.2. Axes' Common Perpendicular and Feet Points

After characterizing the axes and its range of motion, we computed the common perpendicular line and the intersection points (feet) with the estimated axes. The *feet* points will be used for represent the shank-foot-ankle kinematic chain. In this subsection, we use the results from Table S6, Table S8, and Table S9. We compute the common perpendicular from the minimum, maximum, and mean axis attitude from the Table S13.

Table S13. Axes vectors for minimum, mean, and maximum values.

Axis attitude	$\hat{\omega}_1$	$\hat{v}_1$	$\hat{\omega}_2$	$\hat{v}_2$
Minimum	(-0.218, 0.945, 0.242)	(102, 23.5, 0)	(0.703, 0.559, 0.439)	(62.7, -79.9, 1.48)
Mean	(-0.103, 0.979, 0.174)	(106., 11.1, 0)	(0.738, 0.208, 0.642)	(23.2, -84.5, 0.682)
Maximum	(0.0174, 0.994, 0.105)	(107, -1.87, 0)	(0.629, 0.208, 0.749)	(23.1, -72.7, 0.796)

For each group of values, the resulting common perpendicular and feet are in Table S14.

Table S14. Common perpendicular and feet points.

Axis attitude	$\hat{\omega}_c$	$\hat{v}_c$	$\hat{r}_{1c}$	$\hat{r}_{2c}$
Minimum	(0.2796, 0.2658, -0.7862)	(26, -30, -2.4)	(-0.94, 4.1, -110)	(-32, -26, -19)
Mean	(0.5923, 0.1945, -0.7439)	(20, -64, -2.2)	(-0.24, 2.3, -110)	(-51, -14, -44)
Maximum	(0.7227, 0.05301, -0.6216)	(15, -79, 9.2)	(-0.24, -14, -110)	(-54, -18, -63)

Now, we have almost three different configurations through changing the axes' attitude statistical values.

S2.3. Subtalar Axis Range of Motion

The range of motion for the subtalar axis is similar to the talocrural, and the points for the negative angles are in Table S15.

Table S15. Subtalar axis negative angles points.

Sample set *i*	Trajectory A	Trajectory B	Trajectory C
1	(-111.42 6.5037 -183.21)	(42.270 -118.34 -152.38)	(76.602 75.518 -189.75)
2	(-112.41 5.3489 -181.69)	(45.794 -115.24 -157.44)	(73.062 81.010 -187.46)
3	(-113.34 4.1020 -180.21)	(49.150 -111.81 -162.41)	(69.365 86.283 -184.92)
4	(-114.22 2.7668 -178.78)	(52.329 -108.09 -167.27)	(65.520 91.322 -182.13)
5	(-115.03 1.3469 -177.39)	(55.322 -104.06 -172.02)	(661.539 96.111 -179.10)

The points difference in this case is in Table S16.

Table S16. Points differences for the subtalar negative angles.

Sample set *i*	B − A	C − A
1	(153.69 -124.85 30.829)	(188.02 69.014 -6.5481)
2	(158.20 -120.59 24.255)	(185.47 75.661 -5.7695)
3	(162.49 -115.92 17.808)	(182.71 82.181 -4.7012)
4	(166.54 -110.85 11.507)	(179.74 88.555 -3.3472)
5	(170.35 -105.41 5.3694)	(176.56 94.764 -1.7107)

The components for the rotation matrices in this case are in Table S17.

Table S17. Rotation matrices components for the subtalar axis negative angles.

Sample set *i*	Vector $\hat{\mathbf{n}}$	Vector $\hat{\mathbf{s}}$	Vector $\hat{\mathbf{a}}$
1	(-0.0377 0.196 0.980)	(0.984 -0.161 0.0700)	(0.171 0.967 -0.187)
2	(-0.0328 0.156 0.987)	(0.990 -0.129 0.0533)	(0.136 0.979 -0.150)
3	(-0.0264 0.116 0.993)	(0.995 -0.0972 0.0378)	(0.101 0.989 -0.112)
4	(-0.0186 0.0755 0.997)	(0.998 -0.0642 0.0235)	(0.0658 0.995 -0.0741)
5	(-0.00945 0.0356 0.999)	(0.999 -0.0307 0.0105)	(0.0310 0.999 -0.03534)

The rotation matrices for the subtalar axis negative angles are in the Table S18.

Table S18. Subtalar axis negative angles rotation matrices.

Sample set *i*	Rotation matrix	Angle (Rad)
1	$\begin{pmatrix} 0.98449 & 0.17132 & -0.037672 \\ -0.16086 & 0.96740 & 0.19561 \\ 0.069956 & -0.18652 & 0.97996 \end{pmatrix}$	0.26181
2	$\begin{pmatrix} 0.99016 & 0.13607 & -0.032763 \\ -0.12943 & 0.97930 & 0.15560 \\ 0.053258 & -0.14983 & 0.98728 \end{pmatrix}$	0.20838
3	$\begin{pmatrix} 0.99455 & 0.10087 & -0.026412 \\ -0.097195 & 0.98854 & 0.11552 \\ 0.037762 & -0.11232 & 0.99295 \end{pmatrix}$	0.15495
4	$\begin{pmatrix} 0.99766 & 0.065822 & -0.018631 \\ -0.064242 & 0.99507 & 0.075498 \\ 0.023509 & -0.074124 & 0.99697 \end{pmatrix}$	0.10153
5	$\begin{pmatrix} 0.99947 & 0.031024 & -0.0094457 \\ -0.030669 & 0.99889 & 0.035639 \\ 0.010541 & -0.035331 & 0.99932 \end{pmatrix}$	0.048085

The greatest of the negative angles is -0.2618 radians. Table S19 shows the points for the subtalar positive angles.

Table S19. Subtalar axis positive angles trajectories.

Sample set *i*	Trajectory A	Trajectory B	Trajectory C
1	(-116.32 -1.4090 -175.01)	(60.212 -96.112 -180.22)	(54.066 104.06 -173.08)
2	(-116.94 -3.0434 -173.76)	(62.640 -91.324 -184.56)	(49.766 108.08 -169.43)
3	(-117.49 -4.7460 -172.58)	(64.851 -86.289 -188.74)	(45.374 111.81 -165.59)
4	(-117.97 -6.5117 -171.46)	(66.840 -81.021 -192.73)	(40.903 115.23 -161.55)
5	(-118.37 -8.3355 -170.40)	(68.602 -75.534 -196.54)	(36.366 118.33 -157.34)

The points differences are in Table S20.

Table S20. Points difference for the subtalar axis positive angles.

Sample set *i*	B − A	C − A
1	(176.53 -94.703 -5.2102)	(170.38 105.47 1.9314)
2	(179.58 -88.281 -10.798)	(166.70 111.13 4.3313)
3	(182.34 -81.543 -16.158)	(162.86 116.55 6.9919)
4	(184.81 -74.509 -21.276)	(158.87 121.74 9.9048)
5	(186.97 -67.199 -26.137)	(154.74 126.66 13.062)

The rotation matrices components are in Table S21.

Table S21. Components of the rotation matrices for the subtalar axis positive angles.

Sample set *i*	Vector $\hat{\mathbf{n}}$	Vector $\hat{\mathbf{s}}$	Vector $\hat{\mathbf{a}}$
1	(0.0105 -0.0353 0.999)	(0.999 0.0310 -0.00945)	(-0.0307 0.999 0.0356)
2	(0.0235 -0.0741 0.997)	(0.998 0.0658 -0.0186)	(-0.0642 0.995 0.07553)
3	(0.0378 -0.112 0.993)	(0.995 0.101 -0.0264)	(-0.0972 0.989 0.116)
4	(0.0533 -0.150 0.987)	(0.990 0.136 -0.0328)	(-0.129 0.979 0.156)
5	(0.0700 -0.187 0.980)	(0.984 0.171 -0.0377)	(-0.161 0.967 0.196)

The rotation matrices for the subtalar axis positive angles are in Table S22.

Table S22. Rotation matrices for the subtalar axis positive angles.

Sample set *i*	Rotation matrix	Angle (Rad)
1	$\begin{pmatrix} 0.99947 & -0.030669 & 0.010542 \\ 0.031024 & 0.99889 & -0.035329 \\ -0.0094465 & 0.035638 & 0.99932 \end{pmatrix}$	0.048085
2	$\begin{pmatrix} 0.99766 & -0.064241 & 0.023509 \\ 0.065821 & 0.99507 & -0.074124 \\ -0.018631 & 0.075498 & 0.99697 \end{pmatrix}$	0.10153
3	$\begin{pmatrix} 0.99455 & -0.097194 & 0.037759 \\ 0.10087 & 0.98854 & -0.11233 \\ -0.026409 & 0.11552 & 0.99295 \end{pmatrix}$	0.15495
4	$\begin{pmatrix} 0.99016 & -0.12943 & 0.053257 \\ 0.13607 & 0.97930 & -0.14983 \\ -0.032762 & 0.15560 & 0.98728 \end{pmatrix}$	0.20838
5	$\begin{pmatrix} 0.98449 & -0.16086 & 0.069953 \\ 0.17132 & 0.96740 & -0.18652 \\ -0.037669 & 0.19561 & 0.97996 \end{pmatrix}$	0.26180

The greatest positive value is 0.2618 radians. Then the range of motion is 0.5236 radians.

S2.4. Trajectories From the Group of Movements

In this subsection, we use synthetic trajectories generated from the product of exponential matrices. We take 50 samples for each generated trajectory and obtain the plane containing the trajectories. The resulting trajectory for the A is in Figure S11.

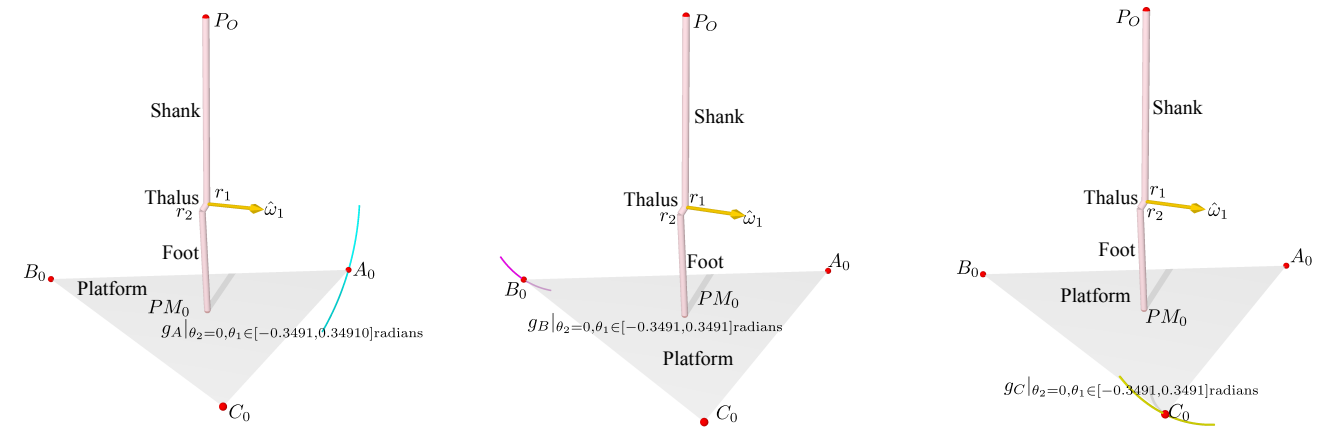

Figure S11. Trajectories for talocrural axis estimation. (**a**) Trajectory A. (**b**) Trajectory B. (**c**) Trajectory C.

We computed the mean rotation axis and the mean axis and center. The rotation axis and trajectory center are in Table S23.

Table S23. Talocrural mean rotation axis and center.

Trajectory estimation	Mean rotation axis	Mean trajectory center
Talocrural joint	(-0.10294, 0.97941, 0.17364)	(0.66912, -11.871, -108.81)

The resulting circle-fitting procedure for the trajectories A, B, and C to compute the talocrural axis model is in Figure S12.

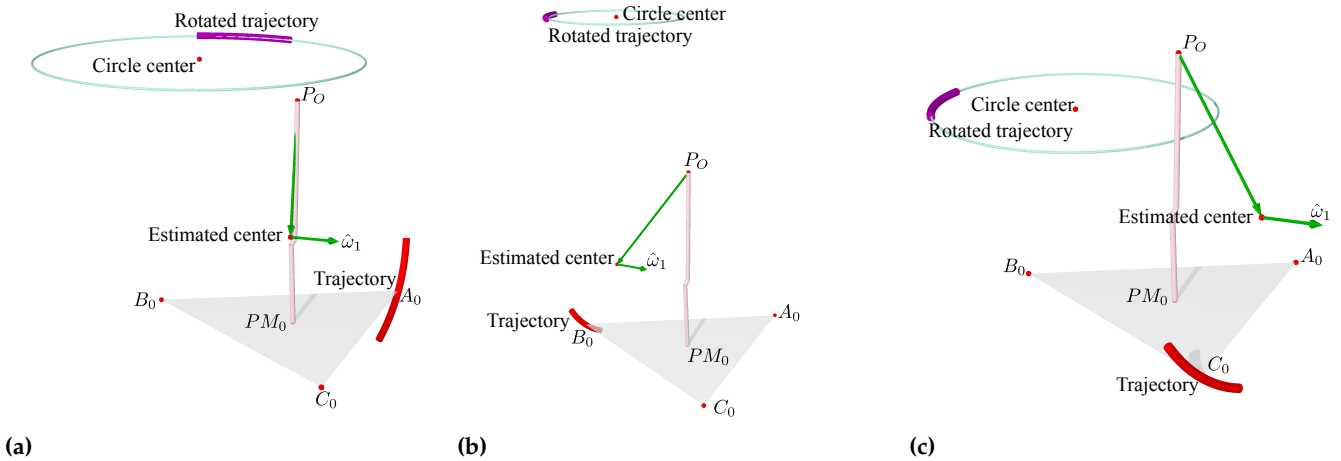

Figure S12. Trajectories for talocrural axis estimation.(**a**) Circle-fitting A. (**b**) Circle-fitting B. (**c**) Circle-fitting C.

We apply a similar method for the subtalar axis estimation. The resulting trajectories generated for the subtalar axis estimation are in Figure S13.

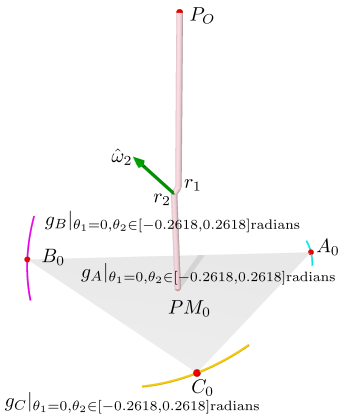

Figure S13. Trajectories for subtalar axis estimation.

Then, we summarized the resulting normal vector, angle, and axis regarding the plane parallel to x-y in Table S24.

Table S24. Plane containing the trajectories A, B, and C for the subtalar axis estimation.

Trajectory	Unitary normal vector	Angle (rad)	Subtalar Axis
A	(0.73827, 0.20787, 0.64167)	0.87412	(0.27102, -0.96257, 0)
B	(0.73823, 0.20790, 0.64171)	0.87407	(0.27108, -0.96256, 0)
C	(0.73821, 0.20789, 0.64174)	0.87404	(0.27107, -0.96256, 0)

The resulting circle-fitting estimation is in Table S25.

Table S25. Circle-fitting for the subtalar axis estimation.

Trajectory	Center parallel to plane x-y	Radius	Estimated center
A	(79.45, 26.55, -198.5)	33.37	(-95.929, -22.830, -191.53)
B	(84.05, 23.25, -91.18)	129.8	(-13.335, -4.1798, -125.39)
C	(84.50, 22.43, -49.52)	130.7	(17.795, 3.6453, -98.822)

The mean rotation axis and mean trajectory center for the talocrural axis are in Table S26.

Table S26. Subtalar mean rotation axis and center.

Trajectory estimation	Mean rotation axis	Mean trajectory center
Talocrural joint	(0.73824, 0.20789, 0.64171)	(-30.490, -7.7882, -138.58)

The resulting circle-fitting procedure for the subtalar axis is in Figure S14.

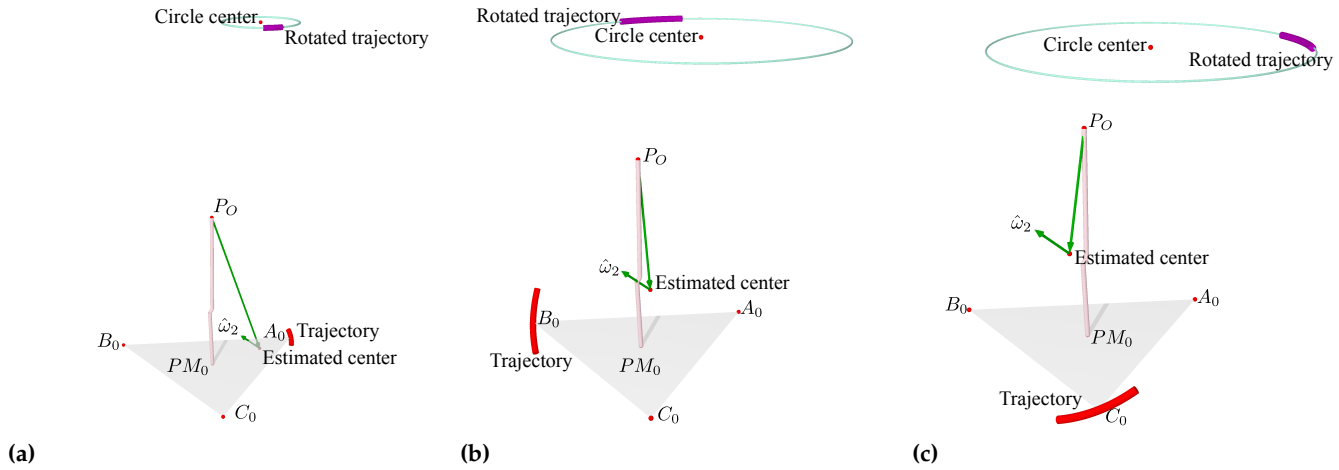

Figure S14. Circle-fitting for the subtalar axis estimation.(**a**) Circle-fitting A. (**b**) Circle-fitting B. (**c**) Circle-fitting C.

We summarized the resulting characterization compared to the provided by the synthetic data and the minimal distance error in Table S27.

Table S27. Axes estimation.

Axis direction vector	Original	Estimated	Absolute error
$\hat{\omega}_1$	(-0.10294, 0.97941, 0.17365)	(-0.10294, 0.97941, 0.17364)	0.0000081395
$\hat{v}_1$	(105.59, 11.098, 0)	(104.51, 11.085, -0.56662)	1.2164
$\hat{\omega}_2$	(0.73822, 0.20791, 0.64172)	(0.73824, 0.20789, 0.64171)	0.000035358
$\hat{v}_2$	(23.199, -84.478, 0.68201)	(23.811, -82.740, -0.58889)	2.2381

S2.5. Talocrural Range of Motion

In this subsection we use decimated data for illustrative purposes. First, we divided the trajectories in two groups. From the initial position reference we separate the negative and the positive angles. The Table S28 shows the negative angle group.

Table S28. Negative angles group.

Sample set *i*	Trajectory A	Trajectory B	Trajectory C
1	(-85.819 9.2808 -210.81)	(72.031 -102.03 -157.42)	(82.714 97.870 -148.31)
2	(-92.897 7.4419 -204.63)	(69.681 -101.54 -161.62)	(78.451 98.546 -154.65)
3	(-99.503 5.5655 -197.97)	(67.039 -101.10 -165.64)	(73.747 99.122 -160.69)
4	(-105.60 3.6610 -190.84)	(64.117 -100.73 -169.48)	(68.628 99.594 -166.39)
5	(-111.17 1.7382 -183.30)	(60.930 -100.42 -173.11)	(63.118 99.960 -171.72)

The points differences for negative angles are in Table S29.

Table S29. Points differences for negative angles.

Sample set *i*	B − A	C − A
1	(157.85 -111.31 53.392)	(168.53 88.589 62.503)
2	(162.58 -108.98 43.017)	(171.35 91.104 49.982)
3	(166.54 -106.66 32.322)	(173.25 93.557 37.278)
4	(169.72 -104.39 21.360)	(174.23 95.933 24.456)
5	(172.10 -102.16 10.188)	(174.29 98.222 11.580)

The rotation matrix vectors components are in Table S30.

Table S30. Rotation matrices vectors components.

Sample set *i*	Vector n̂	Vector ŝ	Vector â
1	(-0.336 -0.0250 0.942)	(0.940 -0.0655 0.334)	(0.0533 0.998 0.0455)
2	(-0.269 -0.0217 0.963)	(0.962 -0.0515 0.268)	(0.0438 0.998 0.0348)
3	(-0.201 -0.0175 0.979)	(0.979 -0.0378 0.201)	(70.0335 0.999 0.0247)
4	(-0.132 -0.0123 0.991)	(0.991 -0.0244 0.132)	(0.0225 1.00 00154)
5	(-0.0628 -0.00625 0.998)	(0.998 -0.0113 0.0627)	(0.0109 1.00 0.00694)

The rotation matrices and the angles are in Table S31.

Table S31. Rotation matrices and angles.

Sample set *i*	Rotation matrix	Angle (Rad)
1	$\begin{pmatrix} 0.94033 & 0.053311 & -0.33606 \\ -0.065472 & 0.99754 & -0.024951 \\ 0.33390 & 0.045465 & 0.94151 \end{pmatrix}$	0.34906
2	$\begin{pmatrix} 0.96206 & 0.043761 & -0.26931 \\ -0.051493 & 0.99844 & -0.021710 \\ 0.26794 & 0.034754 & 0.96281 \end{pmatrix}$	0.27784
3	$\begin{pmatrix} 0.97896 & 0.033475 & -0.20128 \\ -0.037763 & 0.99913 & -0.017498 \\ 0.20052 & 0.024731 & 0.97938 \end{pmatrix}$	0.20659
4	$\begin{pmatrix} 0.99095 & 0.022510 & -0.13233 \\ -0.024354 & 0.99963 & -0.012335 \\ 0.13200 & 0.015446 & 0.99113 \end{pmatrix}$	0.13536
5	$\begin{pmatrix} 0.99797 & 0.010919 & -0.062787 \\ -0.011333 & 0.99992 & -0.0062454 \\ 0.062714 & 0.0069443 & 0.99801 \end{pmatrix}$	0.064138

The greatest negative value is 0.34906 radians. The positive values, which start from the initial position and go through to the trajectory end, are in Table S32.

Table S32. Positive angles group.

Sample set *i*	Trajectory A	Trajectory B	Trajectory C
1	(-119.75 -1.7381 -168.78)	(54.579 -100.03 -179.05)	(52.308 100.35 -180.30)
2	(-123.68 -3.6604 -160.26)	(50.741 -99.914 -181.99)	(45.861 100.41 -184.46)
3	(-126.97 -5.5639 -151.48)	(46.707 -99.865 -184.66)	(39.139 100.36 -188.16)
4	(-129.63 -7.4390 -142.48)	(42.496 -99.885 -187.04)	(32.177 100.20 -191.39)
5	(-131.62 -9.2762 -133.30)	(38.130 -99.975 -189.12)	(25.009 99.927 -194.12)

The points differences for the positive angles are in Table S33.

Table S33. Points differences for positive angles.

Sample set *i*	B − A	C − A
1	(174.33 -98.294 -10.271)	(172.06 102.08 -11.522)
2	(174.42 -96.253 -21.729)	(169.54 104.07 -24.200)
3	(173.68 -94.301 -33.178)	(166.11 105.92 -36.685)
4	(172.12 -92.446 -44.562)	(161.80 107.64 -48.913)
5	(169.75 -90.699 -55.822)	(156.63 109.20 -60.822)

The rotation matrix components are in Table S34.

Table S34. Rotation matrix components for the positive angles.

Sample set *i*	Vector n̂	Vector ŝ	Vector â
1	(0.0627 0.00694 0.998)	(0.998 0.0109 -0.0628)	(-0.0113 1.00 -0.00625)
2	(0.132 0.0154 0.991)	(0.991 0.0225 -0.132)	(-0.0244 1.00 -0.0123)
3	(0.201 0.0247 0.979)	(0.979 0.0335 -0.201)	(-0.0378 0.999 -0.0175)
4	(0.268 0.0348 0.963)	(0.962 0.0438 -0.269)	(-0.0515 0.998 -0.0217)
5	(0.334 0.0455 0.942)	(0.940 0.0533 -0.336)	(-0.0655 0.998 -0.0250)

The rotation matrices for the positive angles are in Table S35.

Table S35. Rotation matrices for the positive angles.

Sample set *i*	Rotation matrix	Angle (Rad)
1	$\begin{pmatrix} 0.99797 & -0.011333 & 0.062715 \\ 0.010919 & 0.99992 & 0.0069439 \\ -0.062788 & -0.0062450 & 0.99801 \end{pmatrix}$	0.064138
2	$\begin{pmatrix} 0.99095 & -0.024354 & 0.13200 \\ 0.022510 & 0.99963 & 0.015445 \\ -0.13232 & -0.012334 & 0.99113 \end{pmatrix}$	0.13536
3	$\begin{pmatrix} 0.97896 & -0.037763 & 0.20052 \\ 0.033475 & 0.99914 & 0.024733 \\ -0.20128 & -0.017500 & 0.97938 \end{pmatrix}$	0.20659
4	$\begin{pmatrix} 0.96206 & -0.051493 & 0.26793 \\ 0.043760 & 0.99844 & 0.034756 \\ -0.26931 & -0.021713 & 0.96281 \end{pmatrix}$	0.27784
5	$\begin{pmatrix} 0.94033 & -0.065471 & 0.33390 \\ 0.053311 & 0.99754 & 0.045464 \\ -0.33606 & -0.024951 & 0.94151 \end{pmatrix}$	0.34906

The greatest positive value is 0.34906. The total range of motion is 0.6981 radians.

S2.6. Robot's Platform and Base Sizes

In this section, we select the platform, the base sizes, and the location of the anchor points for mean values. The body segment is proportional to the human height H=1752 mm. The robot platform and base radius are smaller than the platform and base of the draw-wire sensor system.

We multiply the robot platform radius $r_{pr} = P_f \cdot r_p$ and robot base radius $r_{br} = P_f \cdot r_b$, where Pf is a factor from 50% to 100% of the sensor base and sensor platform.

The range of motion in radians for different proportional values are in Table S36.

Table S36. Base-platform ratio and range of motion in radians.

Base / Platform	**0.5r_p**	**0.6r_p**	**0.7r_p**	**0.8r_p**	**0.9r_p**	**1.0r_p**
0.5r_p	-0.0085	0.0879	0.1808	0.2697	0.3533	0.432
0.6r_p	0.1253	0.2217	0.3147	0.4033	0.4871	0.5657
0.7r_p	0.2386	0.3351	0.428	0.5166	0.6004	0.6791
0.8r_p	0.3346	0.4309	0.5239	0.6126	0.6964	0.7749
0.9r_p	0.4161	0.5124	0.6055	0.6941	0.7779	0.8564
1.0r_p	0.4857	0.5821	0.6751	0.7638	0.8475	0.9261

For H maximum, the angles in radians are in Table S37.

Table S37. Angles in radians for the maximum statistical height.

Base / Platform	**0.5r_p**	**0.6r_p**	**0.7r_p**	**0.8r_p**	**0.9r_p**	**1.0r_p**
0.5r_p	0.0884	0.1911	0.2894	0.3821	0.4688	0.5494
0.6r_p	0.2227	0.3255	0.4238	0.5164	0.6032	0.6838
0.7r_p	0.3349	0.4377	0.536	0.6287	0.7154	0.7959
0.8r_p	0.4288	0.5316	0.6297	0.7226	0.8091	0.8898
0.9r_p	0.5079	0.6107	0.7088	0.8015	0.8882	0.9688
1.0r_p	0.5749	0.6777	0.776	0.8687	0.9554	1.036

For H minimum, the resulting angles in radians are in Table S38.

Table S38. Angles in radians for H minimum.

Base / Platform	**0.5r_p**	**0.6r_p**	**0.7r_p**	**0.8r_p**	**0.9r_p**	**1.0r_p**
0.5r_p	-0.0859	0.0053	0.0939	0.1791	0.2601	0.3365
0.6r_p	0.0467	0.1379	0.2265	0.3115	0.3925	0.4691
0.7r_p	0.1604	0.2517	0.3402	0.4253	0.5063	0.5828
0.8r_p	0.2576	0.3487	0.4374	0.5226	0.6035	0.68
0.9r_p	0.3409	0.432	0.5206	0.6058	0.6868	0.7632
1.0r_p	0.4124	0.5037	0.5924	0.6774	0.7583	0.835

For all three cases, we need at least 0.5236 radians for the angle. Additionally, a proportion near to the sensors or the foot is not desirable, so we selected a proportion of 80% from the base (0.8rb) and platform (0.8rp) of the draw-wire sensor system, then $r_{pr} = 92.5584$ mm. and $r_{br} = 120.326$ mm., which are enough for the population mean height H.

The Figure S15 shows the range for the mean, maximum, and minimum heights with selected base and platform sizes.

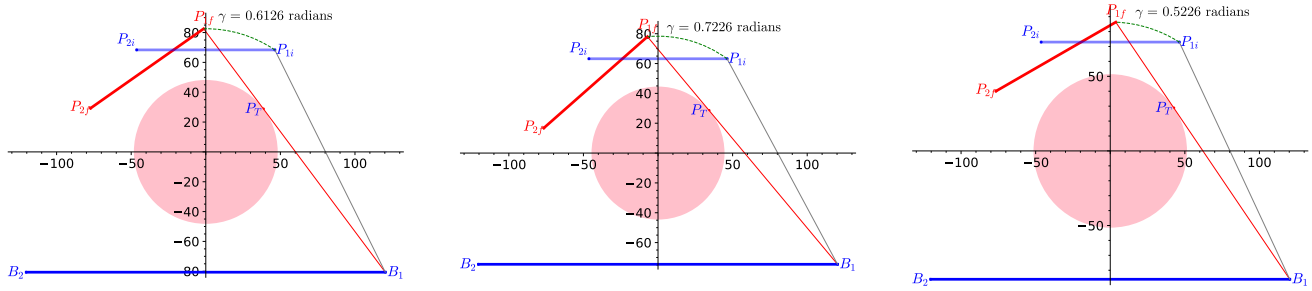

(a) **(b)** **(c)**

Figure S15. Range of motion and platform-base proportions. (**a**) Mean height. (**b**) Maximum height. (**c**) Minimum height.

S2.7. Screws and Reciprocity Initial Analysis

In this subsection, we analyze the platform screws system. We built a model based on the cable anchor with the platform and base. Following that, we reconfigured the anchor point places to 0.7854 radians rotation about the z unitary axis $\hat{k}$. The base and platform corresponding points are provided in the table S39.

Table S39. Point positions at equilibrium.

Points	$\mathbf{P_1}, (\mathbf{x}, \mathbf{y})$	$\mathbf{P_2}, (\mathbf{x}, \mathbf{y})$	$\mathbf{P_3}, (\mathbf{x}, \mathbf{y})$	$\mathbf{P_4}, (\mathbf{x}, \mathbf{y})$
Platform, z=-137.8	(65.45,65.45)	(-65.45,-65.45)	(65.45,-65.45)	(-65.45,65.45)
Base, z=0	(85.08,85.08)	(-85.08,-85.08)	(85.08,-85.08)	(-85.08,85.08)

The resulting reciprocals are in table S40.

Table S40. Reciprocal products.

$\$_{mn} \circ \$_i$	$\$_1$	$\$_2$	$\$_3$	$\$_4$	$\sum(\$_{mn} \circ \$_i)$
$\$_{12}$	6635.7	-6635.7	6635.7	-6635.7	0
$\$_{34}$	6218.6	-6218.6	-6218.6	6218.6	0

We observe that in the $\pi/4$ radians rotated configuration, each pair of cable-driven actuators work in the tensegrity mode. Additionally, it is possible to apply work from the cables in the tension to the rotation axes in the serial kinematic chain.

S2.8. Projection of the Intersection Pivot Point

The projected axis on the plane x-y has a intersection point. We used the different axis attitudes for finding the intersection point. The results are in Table S41.

Table S41. Projected axes intersection point.

Axis attitude	**Base intersection point**	**Platform intersection point**
Minimum	(0.4040, -1.746, 0)	(0.4040, -1.746, -176.2)
Mean	(0.09698, -0.9111, 0)	(0.09698, -0.9111, -176.2)
Maximum	(-0.02179, -1.267, 0)	(-0.02179, -1.267, -176.2)

S2.9. Robot Configuration

We show how to align the robot at the initial projected pivot point intersection. It is imperative to align the references before placing the cable anchors on the platform and the

base. For simulation, we used the ankle forward kinematics, common perpendicular, and range of motion in the S2.1, S2.2 S2.3 sections.
The pivot center point depends on the anthropometric measurements; in this case, we used the standard deviation and the mean values for the common perpendicular distance Q=mean. The resulting projection points are in Table S42.

Table S42. Subtalar and talocrural projection points.

Axis attitude	**TC mean** (x_p, y_p)	**TC+sd** (x_p, y_p)	**TC-sd**(x_p, y_p)
ST mean	(0.0943,-0.8973)	(-0.0162,-0.9284)	(0.2002,-0.8674)
ST+sd	(0.1286,-1.224)	(-0.0222,-1.2739)	(0.2716,-1.1767)
ST-sd	(0.20441 -1.9448)	(-0.037303 -2.1371)	(0.41105 -1.7805)

For Q maximum, we show the results in Table S43.

Table S43. Projected axes intersection point for Q maximum.

Axis attitude	**TC mean** (x_p, y_p)	**TC+sd** (x_p, y_p)	**TC-sd**(x_p, y_p)
ST mean	(0.15090 -1.4357)	(-0.025929 -1.4855)	(0.32043 -1.3879)
ST+sd	(0.20584 -1.9585)	(-0.035578 -2.0383)	(0.43467 -1.8828)
ST-sd	(0.32705 -3.1117)	(-0.059684 -3.4193)	(0.65768 -2.8487)

For Q minimum, the results are in Table S44.

Table S44. Projected axes intersection point for Q minimum.

Axis attitude	**TC mean** (x_p, y_p)	**TC+sd** (x_p, y_p)	**TC-sd**(x_p, y_p)
ST mean	(0.037724 -0.35892)	(-0.0064823 -0.37137)	(0.080107 -0.34698)
ST+sd	(0.051460 -0.48961)	(-0.0088946 -0.50957)	(0.10867 -0.47070)
ST-sd	(0.081764 -0.77793)	(-0.014921 -0.85483)	(0.16442 -0.71219)

We note that by changing the different parameters, the robot has sufficient range to reconfigure the anchor points. Therefore, the aligning system works with different axis attitudes.

S2.10. Angle Computation of the Anchor Points

After we centered the robot around the intersection of the talocrural and subtalar axes projected on the base and initial platform planes, we configured the four cable anchor points. Also, we only changed the axis attitudes and then computed the anchor points. The table S45 shows the resulting computed data for the axes' mean, maximum, and minimum attitude values. We refer to the axes' mean attitude when TC and ST have mean statistical values. Also, we call the maximal attitude when we add the standard deviation to the TC and ST means. The same goes for the minimum.

Table S45. Anchor point computation at initial position.

Computed variables	TC Mean attitude	Maximum	Minimum
$(\hat{\omega}_1)$	(-0.103, 0.979, 0.174)	(0.0174, 0.994, 0.105)	(-0.218, 0.945, 0.242)
$(\hat{v}_1)$	(106, 11.1, 0)	(107, -1.87, 0)	(102, 23.5, 0)
$(\hat{\omega}_2)$	(0.738, 0.208, 0.642)	(0.629, 0.208, 0.749)	(0.703, 0.559, 0.439)
$(\hat{v}_2)$	(23.2, -84.5, 0.682)	(23.1, -72.7, 0.796)	(62.7, -79.9, 1.48)
ϕ_1(rad)	0.70045	0.61696	0.56287
ϕ_2(rad)	0.87035	0.95383	1.0079
Vector 1	(814.89, -552.28)	(800.68, -589.28, 0)	(915.54, -319.9, 0)
Vector 2	(-430.17, -634.71)	(-392.70, -533.57, 0)	(-296.26, -847.89, 0)
Ap1	(-76.52, 51.02,-176.2)	(-74.45, 53.95, -176.2)	(-87.28, 29.62, -176.2)
Ap2	(76.72, -52.84,-176.2)	(74.64, -55.78, -176.2)	(87.47, -31.44, -176.2)
Ap3	(52.03, 75.71,-176.2)	(54.96, 73.63, -176.2)	(30.63, 86.47, -176.2)
Ap4	(-51.83, -77.53,-176.2)	(-54.77, -75.46,-176.2)	(-30.43, -88.29,-176.2)
Ab1	(-99.51, 66.59, 0)	(-96.81, 70.41, 0)	(-113.5, 38.78, 0)
Ab2	(99.70, -68.42, 0)	(97.00, -72.23, 0)	(113.7, -40.60, 0)
Ab3	(67.60, 98.69, 0)	(71.42, 96.00, 0)	(39.79, 112.7, 0)
Ab4	(-67.41, -100.5, 0)	(-71.23, -97.82, 0)	(-39.59, -114.5, 0)

From this table, we computed the angle configuration of the attaching points in table S46.

Table S46. Configuration angle from x direction.

Attitude	α_1	α_2	α_3	α_4
Mean (rad)	2.554	-0.603	0.969	-2.16

The angles for the base and platform anchor points for maximum attitude are in Table S47.

Table S47. Configuration angle from x direction for maximum attitude.

Attitude	α_1	α_2	α_3	α_4
Mean (rad)	2.5145	-0.64173	0.9296	-2.1986

The angles for the base and platform anchor points for maximum attitude are in Table S48.

Table S48. Configuration angle from x direction for minimum attitude.

Attitude	α_1	α_2	α_3	α_4
Mean (rad)	2.8144	-0.34505	1.2304	-1.9027

The Figure S16 shows the anchor points the three axes attitude groups.

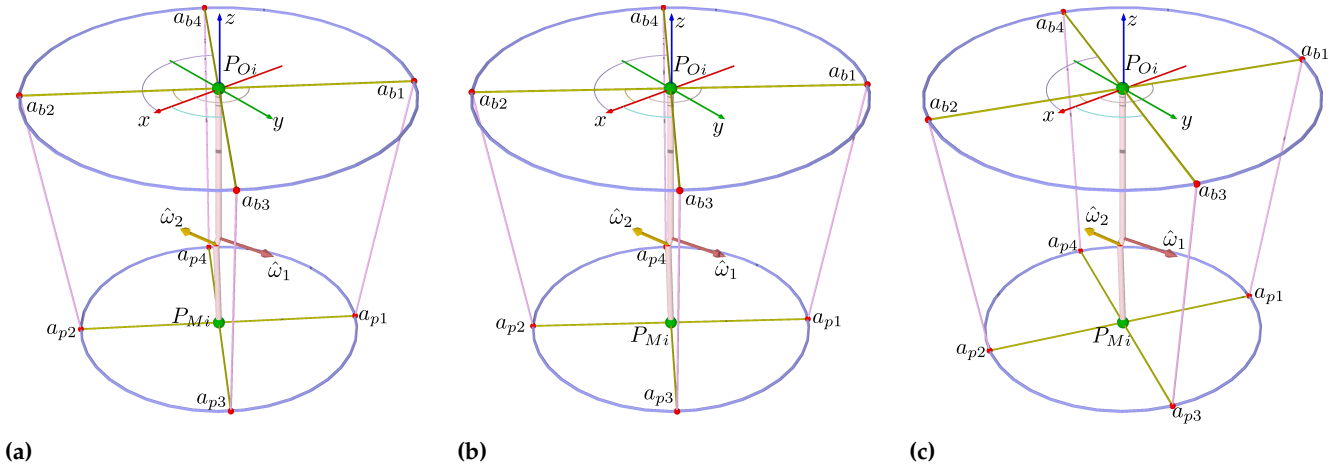

(a) **(b)** **(c)**

Figure S16. Anchor points at initial position. (**a**) Mean statistical attitude. (**b**) Maximum statistical attitude. (**c**) Minimum statistical attitude.

S2.11. Workspace

The workspace is limited by the range of motion of the ankle joint. We computed the different groups of movements shown in Figure S17a.

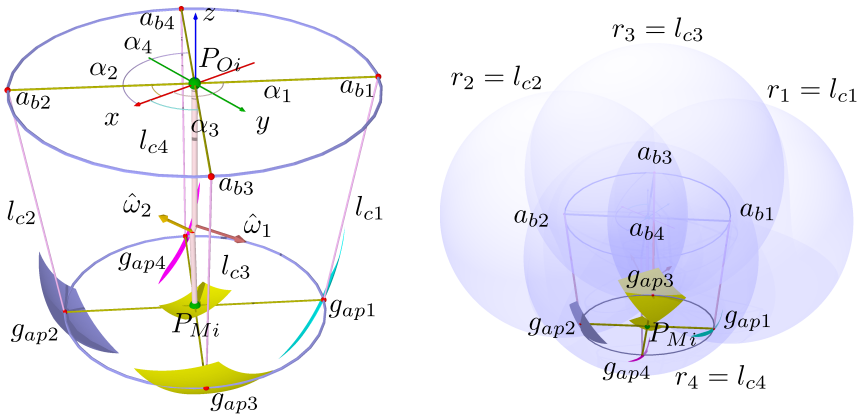

(a) **(b)**

Figure S17. Robot kinematics. (**a**) Centering the platform. (**b**)Forward kinematics.

S2.12. Cable Lengths at Initial Position

We computed the cable lengths at the initial position.
The resulting lengths for the mean values are shown in the table S49.

Table S49. Cable lengths at initial position.

(θ_1, θ_2), radians	lc_1, mm	lc_2, mm	lc_3, mm	lc_4, mm
$(0, 0)$	178.35	178.35	178.35	178.35

For the initial lengths, we drew the forward kinematics in the intersection between four spheres and the circle representing the platform, with the pose represented on $g_{PM(0)}$, as in the Figure S17b.

S2.13. Cable Lengths at Extreme Positions

We created three tables with different axis attitudes and computed the positions. The table S50 shows r_{2_i} and P_{M_i}.

Table S50. Rotation center r_{2i} and PM_i for extreme angles corresponding to axes' mean attitude values.

(θ_1, θ_2), radians	r_{2i}	P_{M_i}
$(-0.3491, -0.2618)$	(4.130, -0.2039, -110.8)	(24.31, -10.56, -170.9)
$(-0.3491, 0.2618)$	(4.130, -0.2039, -110.8)	(18.91, 13.42, -171.8)
$(0.3491, -0.2618)$	(1.361, -0.1503, -112.7)	(-19.34, -15.01, -171.7)
$(0.3491, 0.2618)$	(1.361, -0.1503, -112.7)	(-27.31, 8.175, -169.6)

The table S51 shows the anchor points ap_1, ap_2, ap_3, and ap_4.

Table S51. Anchor points ap_1, ap_2, ap_3, and ap_4 for extreme angles corresponding to axes' mean attitude values.

(θ_1, θ_2), radians	ap_1, mm	ap_2, mm	ap_3, mm	ap_4, mm
$(-0.3491, -0.2618)$	(-30.03, 55.68, -204.3)	(78.32, -78.59, -137.2)	(91.65, 50.21, -156.4)	(24.308, -10.561, -170.9)
$(-0.3491, 0.2618)$	(-62.04, 54.72, -185.9)	(100.3, -29.63, -157.9)	(55.68, 92.49, -142.9)	(-17.38, -67.40, -200.9)
$(0.3491, -0.2618)$	(-90.97, 42.28, -164.9)	(52.40, -74.07, -178.1)	(33.27, 52.65, -204.8)	(-71.83, -84.44, -138.2)
$(0.3491, 0.2618)$	(-103.9, 40.46, -130.3)	(49.78, -25.83, -209.4)	(8.315, 92.79, -172.7)	(-62.48, -78.16, -167.0)

The table S52 lengths for the cables.

Table S52. Cable lengths lc_1, lc_2, lc_3, and lc_4 for extreme angles corresponding to axes' mean attitude values.

(θ_1, θ_2), radians	lc_1, mm	lc_2, mm	lc_3, mm	lc_4, mm
$(-0.3491, -0.2618)$	216.09	139.28	165.48	188.75
$(-0.3491, 0.2618)$	190.06	162.63	143.57	209.71
$(0.3491, -0.2618)$	166.87	184.39	212.67	139.23
$(0.3491, 0.2618)$	133.02	219.41	182.69	168.58

The Figure S18 shows the four configurations corresponding to axes' mean attitude values.

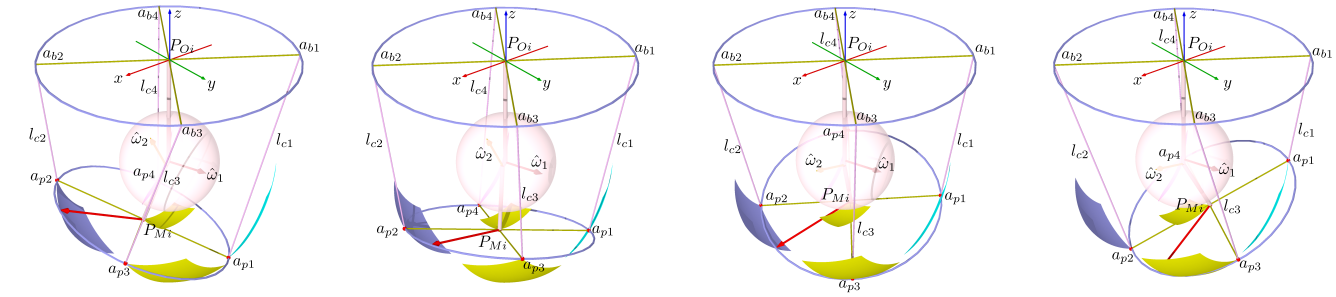

(a) **(b)** **(c)** **(d)**

Figure S18. Configurations for axes' mean attitude values. **a**) Minimal TC and ST angles. (**b**)Minimal TC and ST maximal angles. **c**) Maximal TC and maximal ST angles. (**b**) TC and ST maximal angles.

The resulting platform position anchor points corresponding to the axes' maximum attitude values are in Table S53.

Table S53. Anchor points ap_1, ap_2, ap_3, and ap_4 for extreme angles corresponding to the axes' maximum attitude values.

$(\boldsymbol{\theta_1}, \boldsymbol{\theta_2})$, radians	$\boldsymbol{ap_1}$, mm	$\boldsymbol{ap_2}$, mm	$\boldsymbol{ap_3}$, mm	$\boldsymbol{ap_4}$, mm
$(-0.3491, -0.2618)$	(-27.37, 58.02, -203.7)	(75.66, -80.94, -137.8)	(93.70, 47.56, -155.1)	(-45.41, -70.47, -186.5)
$(-0.3491, 0.2618)$	(-60.56, 57.79, -184.8)	(98.87, -32.70, -159.1)	(58.81, 90.79, -142.4)	(-20.50, -65.70, -201.5)
$(0.3491, -0.2618)$	(-88.87, 44.90, -166.2)	(50.31, -76.69, -176.8)	(36.01, 50.34, -205.0)	(-74.58, -82.13, -138.0)
$(0.3491, 0.2618)$	(-102.5, 43.75, -130.5)	(48.34, -29.12, -209.2)	(11.27, 91.44, -174.2)	(-65.44, -76.81, -165.5)

The cable lengths corresponding to the axes' maximum attitude values are in Table S54.

Table S54. Cable lengths lc_1, lc_2, lc_3, and lc_4 for extreme angles corresponding to the axes' maximum orientation values.

$(\boldsymbol{\theta_1}, \boldsymbol{\theta_2})$, radians	$\boldsymbol{lc_1}$, mm	$\boldsymbol{lc_2}$, mm	$\boldsymbol{lc_3}$, mm	$\boldsymbol{lc_4}$, mm
$(-0.3491, -0.2618)$	215.61	139.75	164	190.24
$(-0.3491, 0.2618)$	188.76	163.92	143.07	210.22
$(0.3491, -0.2618)$	168.3	182.95	212.98	138.93
$(0.3491, 0.2618)$	133.3	219.1	184.38	166.92

The Figure S19 shows the four configurations corresponding to the axes' maximum attitude values.

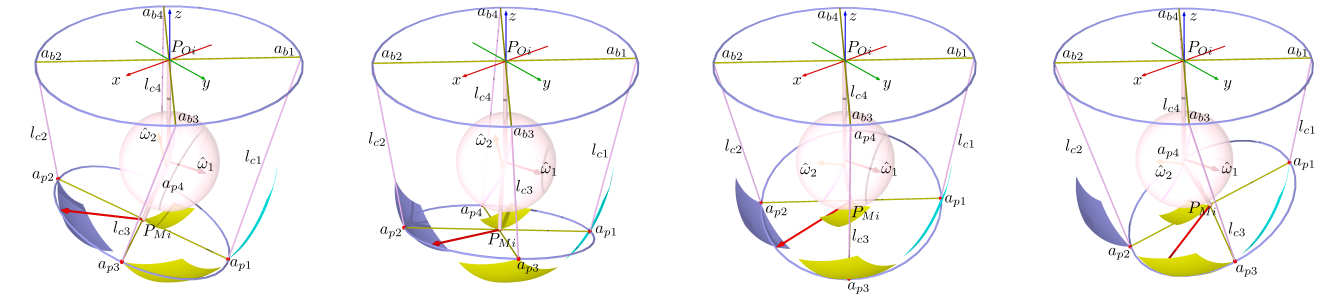

(a) **(b)** **(c)** **(d)**

Figure S19. Configurations corresponding to the axes' maximum attitude values. **a**) Minimal TC and ST angles. (**b**)Minimal TC and ST maximal angles. **c**) Maximal TC and maximal ST angles. (**b**) TC and ST maximal angles.

The resulting platform position anchor points corresponding to the axes' minimum attitude values are in Table S55.

Table S55. Anchor points ap_1, ap_2, ap_3, and ap_4 for extreme angles corresponding to the axes' minimum attitude values.

$(\boldsymbol{\theta_1}, \boldsymbol{\theta_2})$, radians	$\boldsymbol{ap_1}$, mm	$\boldsymbol{ap_2}$, mm	$\boldsymbol{ap_3}$, mm	$\boldsymbol{ap_4}$, mm
$(-0.3491, -0.2618)$	(-45.54, 37.61, -206.9)	(93.82, -60.52, -134.7)	(75.49, 65.37, -165.5)	(-27.20, -88.28, -176.1)
$(-0.3491, 0.2618)$	(-68.69, 32.80, -192.9)	(107.0, -7.706, -151.0)	(33.63, 100.6, -147.5)	(4.678, -75.55, -196.4)
$(0.3491, -0.2618)$	(-102.1, 22.74, -156.6)	(63.49, -54.54, -186.4)	(13.12, 65.28, -201.9)	(-51.68, -97.07, -141.0)
$(0.3491, 0.2618)$	(-110.5, 17.42, -130.9)	(56.29, -2.786, -208.8)	(-12.59, 98.43, -162.5)	(-41.58, -83.80, -177.2)

The cable lengths corresponding to the axes' minimum attitude values are in Table S56.

Table S56. Cable lengths lc_1, lc_2, lc_3, and lc_4 for extreme angles corresponding to the axes' minimum attitude values.

$(\boldsymbol{\theta_1}, \boldsymbol{\theta_2})$, radians	$\boldsymbol{lc_1}$, mm	$\boldsymbol{lc_2}$, mm	$\boldsymbol{lc_3}$, mm	$\boldsymbol{lc_4}$, mm
$(-0.3491, -0.2618)$	217.78	137.59	175.76	178.48
$(-0.3491, 0.2618)$	198.15	154.65	148.13	205.04
$(0.3491, -0.2618)$	157.79	193.59	209.14	142.63
$(0.3491, 0.2618)$	132.71	219.8	171.29	179.9

The Figure S20 shows the four configurations corresponding to the axes' minimum attitude values.

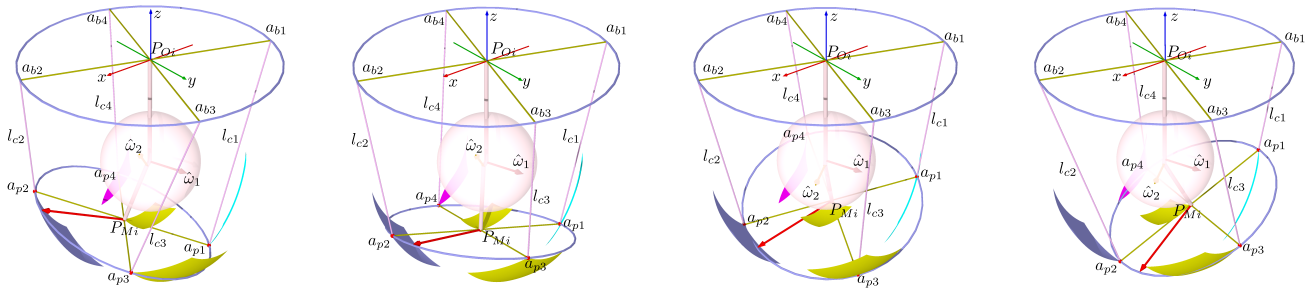

(a) **(b)** **(c)** **(d)**

Figure S20. Configurations for the axes' minimum attitude values. **a**) Minimal TC and ST angles. (**b**)Minimal TC and ST maximal angles. **c**) Maximal TC and maximal ST angles. (**b**) TC and ST maximal angles.

S2.14. MuJoCo Simulations

In this section, we replace the anchor points, the kinematic chain, and the tendon lengths in the XML script for MuJoCo simulations. In the simulation, we rotated 1.5708 radians about the y-axis and scaled the positions by a factor of 0.1. The units are in centimeters. The input values are in table S57.

Table S57. Data for MuJoCo.

Identification	Value
Reference	0 -0.0911 17.6273
base cylinder fromto	-0.4 -0.0911 17.6273 0 -0.0911 17.6273
b1	0 6.6595 7.6668
b2	0 -6.8417 27.5878
b3	0 9.8694 24.3779
b4	0 -10.0516 10.8767
leg capsule fromto	0 -0.0911 17.6273 10.8442 -0.1037 17.6286
shnk pos	0 10.8442 -0.1037 17.6286
comp capsule fromto	10.8442 -0.1037 17.6286 11.1964 -0.0117 17.909
TC hinge pos, axis	110.8442 -0.1037 17.6286, -0.174 0.979 -0.103
b-foot capsule fromto	11.1964 -0.0117 17.909 17.6176 -0.0911 17.6273
ST hinge pos, axis	-0.0117 17.909, -0.642 0.208 0.738
ptfm cylinder fromto	17.6176 -0.0911 17.627 18.0176 -0.0911 17.6273
a-foot refpos	-10.8442 0.1037 -17.6286
p1	17.6176 5.1016 9.9653
p2	17.6176 -5.2838 25.2893
p3	17.6176 7.57 22.82
p4	17.6176 -7.753 12.4345
t1 range	17.83503 17.83513
t2 range	17.83503 17.83513
t3 range	17.83503 17.83513
t4 range	17.83503 17.83513

We put this model the XML document as in the Listing S2.14.

Listing 1: XML MuJoCo file.

```
<?xml version="1.0" encoding="UTF-8"?>
<mujoco model="turmellbot">
  <compiler coordinate="local"/>
  <default>
    <geom rgba=".8␣.6␣.4␣1"/>
  </default>
  <asset>
```

```
  <texture type="skybox" builtin="gradient" rgb1="1␣1␣1" rgb2=".6␣.8␣1"
      width="256" height="256"/>
  <mesh file="a-foot.stl" refpos="-10.84427␣0.1037934␣-17.62868" refquat="
      0.99619␣0.034862␣0.00000␣0.00000"/>
</asset>
<worldbody>
  <light pos="10␣-10␣50" dir="-10␣10␣-50" diffuse="1␣1␣1"/>
  <site name="reference" pos="5.938405e-19␣-0.09110710␣17.62735"/>
  <body>
    <geom name="base" type="cylinder" fromto="-0.4000000␣-0.09110710␣
        17.62735␣5.938405e-19␣-0.09110710␣17.62735" size="12.032592"/>
    <site name="b1" pos="-6.093131e-16␣6.659522␣7.666812" size="0.2"/>
    <site name="b2" pos="6.105008e-16␣-6.841736␣27.58788" size="0.2"/>
    <site name="b3" pos="4.139506e-16␣9.869429␣24.37798" size="0.2"/>
    <site name="b4" pos="-4.127630e-16␣-10.05164␣10.87672" size="0.2"/>
    <geom name="leg" type="capsule" fromto="5.938405e-19␣-0.09110710␣
        17.62735␣10.84427␣-0.1037934␣17.62868" size="0.3"/>
    <site name="shnk" pos="10.84427␣-0.1037934␣17.62868"/>
    <body>
      <geom name="comp" type="capsule" fromto="10.84427␣-0.1037934␣17.62868
          ␣11.19642␣-0.01170672␣17.90907" size="0.3"/>
      <joint name="TC" type="hinge" pos="10.84427␣-0.1037934␣17.62868" axis
          ="-0.1740000␣0.9790000␣-0.1030000" limited="true" range="-20␣20"/
          >
      <body>
        <geom name="b-foot" type="capsule" fromto="11.19642␣-0.01170672␣
            17.90907␣17.61765␣-0.09110710␣17.62735" size="0.3"/>
        <joint name="ST" type="hinge" pos="11.19642␣-0.01170672␣17.90907"
            axis="-0.6420000␣0.2080000␣0.7380000" limited="true" range="-15
            ␣15"/>
        <geom name="ptfm" type="cylinder" fromto="17.61765␣-0.09110710␣
            17.627␣18.01765␣-0.09110710␣17.62735" size="9.25584"/>
        <site name="ptfmc" pos="18.01765␣-0.09110710␣17.62735" size="0.3"/>
        <geom name="s-foot" type="mesh" mesh="a-foot" rgba=".85␣.79␣.72␣0.7
            " density="0.01"/>
        <site name="p1" pos="17.61765␣5.101684␣9.965397" size="0.2"/>
        <site name="p2" pos="17.61765␣-5.283899␣25.28930" size="0.2"/>
        <site name="p3" pos="17.61765␣7.570844␣22.82014" size="0.2"/>
        <site name="p4" pos="17.61765␣-7.753058␣12.43456" size="0.2"/>
      </body>
    </body>
  </body>
</worldbody>
<tendon>
  <spatial name="t1" limited="true" range="17.83503␣17.83513" width="0.05"
      stiffness="100" damping="100000">
    <site site="b1"/>
    <site site="p1"/>
  </spatial>
  <spatial name="t2" limited="true" range="17.83503␣17.83513" width="0.05"
      stiffness="100" damping="100000">
    <site site="b2"/>
    <site site="p2"/>
  </spatial>
  <spatial name="t3" limited="true" range="17.83503␣17.83513" width="0.05"
      stiffness="100" damping="100000">
    <site site="b3"/>
    <site site="p3"/>
  </spatial>
  <spatial name="t4" limited="true" range="17.83503␣17.83513" width="0.05"
      stiffness="100" damping="100000">
    <site site="b4"/>
    <site site="p4"/>
  </spatial>
</tendon>
<actuator>
  <muscle name="t1" tendon="t1"/>
  <muscle name="t2" tendon="t2"/>
  <muscle name="t3" tendon="t3"/>
```

```
    <muscle name="t4" tendon="t4"/>
  </actuator>
  <sensor>
    <accelerometer name="ptfacc" site="ptfmc"/>
    <gyro name="ptfgyro" site="ptfmc"/>
    <tendonpos name="t1pos" tendon="t1"/>
    <tendonpos name="t2pos" tendon="t2"/>
    <tendonpos name="t3pos" tendon="t3"/>
    <tendonpos name="t4pos" tendon="t4"/>
    <jointpos name="TCpos" joint="ST"/>
    <jointpos name="STpos" joint="TC"/>
  </sensor>
</mujoco>
```

There are bodies such as the base and the platform, three links, two hinge joints, and four tendons with sensors and actuators. The data configuration is from the simulation at the initial position. We saved the file with XML format, then dragged and dropped them in Simulate, and the resulting screenshot is in Figure S21.

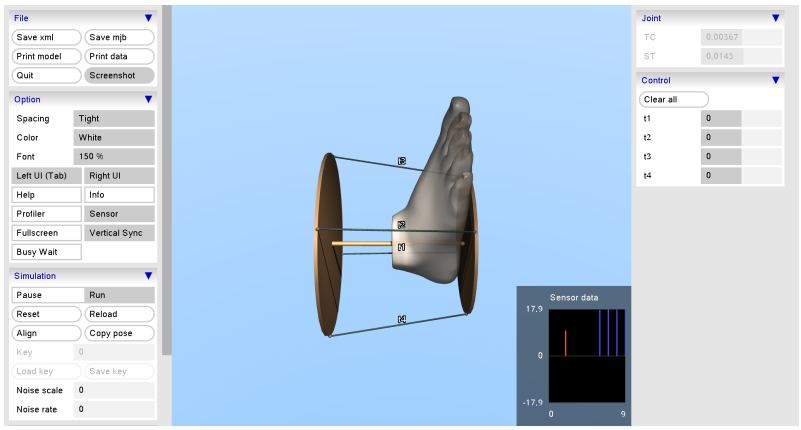

Figure S21. Simulation at initial position.

The sensors in the print data button from MuJoCo generate the MJDATA.txt file, which contains the sensor measurements. We put the sensors ouptut in table S58.

Table S58. Sensors output in MuJoCo.

Sensor	Measurement
Accelerometer at the platform	-0.065 -0.096 9.8
Gyro at the platform	3.4e-14 -2.7e-13 4e-14
Length tendon 1	18
Length tendon 2	18
Length tendon 3	18
Length tendon 4	18
Talocrural joint in radians	0.014
Subtalar joint in radians	0.0037

Regarding the minimum and maximum values, we stopped the simulation, changing the range of the tendons and moving the joints sliders to the minimum angles.

Table S59. Changes on tendon lengths.

Configuration N	t1,t2,t3,t4, (input, cm)	Acc.	Gyr.	t1,t2,t3,t4, (output, cm)	TC(rad)	ST(rad)
1	21.6, 13.92, 16.54, 18.87	3.4 2.5 8.8	0,0,0	21,14,17,19	-0.24	-0.34
2	19, 16.26, 14.35, 20.96	2.6 -1.5 9.3	0,0,0	19,16,14,21	0.25	-0.34
3	16.68, 18.43, 21.26, 13.92	-2.7 0.35 9.4	0,0,0	17,18,21,14	-0.25	0.34
4	13.3, 21.94, 18.26, 16.85	-3.9 -1.4 8.9	0,0,0	13,18,18,17	0.25	0.34

* Accelerations approximately g=norm(Acc.)=9.8 m/s^2 and angles in radians.

Snapshots of the different configurations are in Figure S22.

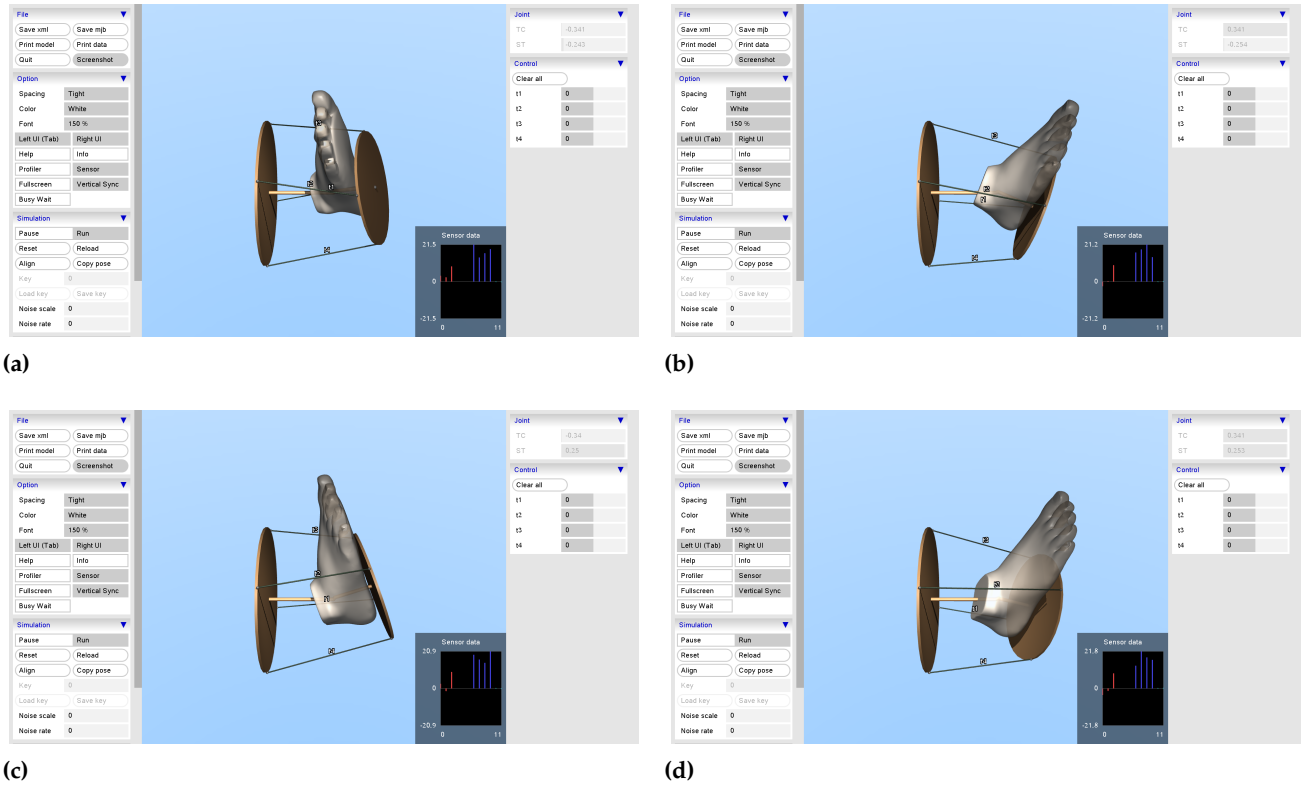

Figure S22. Snapshots of MuJoCo Simulate with extreme angles configurations. **a**) Minimal TC and ST angles. (**b**)Maximal TC and ST minimal angles. **c**) Minimal TC and maximal ST angles. (**b**) TC and ST maximal angles.